Basin Research
February 2022, Volume 34, Issue 1, Pages 24-49
https://doi.org/10.1111/bre.12609
https://archimer.ifremer.fr/doc/00718/83045/

Tectono- stratigraphic evolution of the offshore western Niger Delta from the Cretaceous- present: Implications of delta dynamics and paleo- topography on gravity- driven deformation.

Chima Kelvin Ikenna [1, 2, *], Granjeon Didier [3], Do Couto Damien [1], Leroux Estelle [4], Gorini Christian [1], Rabineau Marina [5], Letouzey Jean [1], Hoggmascall Nick [6], Glukstad Miguel-mora [7]

[1] Sorbonne Université-ISTeP UMR 7193 F75000 Paris, France
[2] Alex Ekwueme Federal University Ndufu-Alike P.M.B. 1010 Ebonyi State, Nigeria
[3] IFPEN Rueil-Malmaison, France
[4] IFREMER ZI Pointe du Diable Plouzane, France
[5] CNRS, Univ Brest, Univ. Bretagne-Sud, Laboratoire Géosciences Océan (LGO), UMR6538, IUEM rue Dumont d'Urville F-29280 Plouzané, France
[6] Brunei Shell Petroleum Sendirian Berhad, Jalan Utara, Panaga, Seria, KB2933
[7] Ras Al Hamra Petroleum Development Oman (PDO), oman

* Corresponding author : Kelvin Ikenna Chima, email addresses : kelvin.chima@funai.edu.ng ; kelvini.chima@gmail.com

Abstract :

The interaction between sedimentary wedge dynamics and paleo-fracture zones is investigated offshore Western Niger Delta lobe (WNDL) to reconstruct the evolution of the delta from the Cretaceous to present. This was achieved through detailed regional seismic interpretation, calibrated with well data.

Our results suggest that high sedimentation rates in the WNDL since the Serravallian-Tortonian triggered the migration of the 'Oligocene-Tortonian extensional zone' and gravity spreading seawards (from a present-day onshore to a present-day offshore position), with extensional, translational and contractional deformation. An additional increase in sedimentation rate since the early Pliocene, further accelerated gravity spreading and the development of the present-day contractional front. A five-stage tectono-stratigraphic evolution of the offshore WNDL from the late Cretaceous-present is proposed.

Paleo-topographies formed by the Charcot and Chain Fracture Zones, exerted depositional control on the stratigraphic architecture of the offshore WNDL from the Cretaceous to Serravallian. Differential subsidence on both sides of the relict Charcot and Chain transform faults is responsible for the segmentation of gravity-driven deformation of the eastern and western Niger Delta lobes.

In addition, a comparison of the stratigraphic architecture of the Eastern Niger Delta Lobe (ENDL) and WNDL demonstrates a similar overall progradation and sediment bypass to the deep basin during the Pliocene. During the Pleistocene, the two lobes show a distinct evolution and architecture: the ENDL shows an overall retrogradation and sediment sequestration on the shelf whereas the WNDL displays an

overall progradation and sediment bypass. This study documents long-term and large-scale control of delta dynamics and paleo-topography on gravity-driven deformation of the offshore eastern and western Niger Delta lobes, and similar analysis could be applied in the reconstruction of other passive margin basins.

Keywords : Delta dynamics, Gravity spreading, Paleo-topography, Sedimentary wedge deformation, Stratigraphic architecture, The Niger Delta

1. Introduction

The Cenozoic Niger Delta is a prolific petroleum province, fed by a large progradational delta along a passive continental margin. The Niger Delta is characterised by gravity-driven deformation of a sedimentary wedge above overpressured marine shales (Doust and Omasola, 1990; Damuth, 1994; Cohen and McClay, 1996; Fig. 1). The siliciclastic wedge of the Niger Delta is ~12 km thick, and displays concave, divergent seaward lobate geometry in plan view (Fig. 1B). The main pulse of deltaic sedimentation started in the late Eocene and the delta front has prograded ~300 km seaward of the modern coastline (Fig. 1B, C). Gravity-driven deformation of the Niger Delta wedge is characterised by delta-top extensional faults in the proximal setting and imbricated fold-thrust faults that detach within overpressured marine shales in the distal setting (Fig. 1B, C).

The offshore Niger Delta is segmented into the ENDL and WNDL by stepped oceanic basement, formed by the Charcot Fracture Zone (Short and Stauble, 1967; Evamy *et al.,* 1978; Wu *et al.,* 2015; Fig. 1A, B). The ENDL and WNDL are in turn underlain by Fernando Po and Chain Fracture Zones, respectively (Fig. 1A, B). These fracture zones were active transform faults in the middle Aptian, during the opening of the equatorial Atlantic, but were fossilised in the Santonian, when oceanic spreading began to slow-down (Lehner and de Ruiter, 1977; Briggs *et al.,* 2009). Although analogue modelling of the offshore Niger Delta by Wu *et al.* (2015), documented differential sediment thickening across the relict Chain and Charcot Fracture Zones, the long-term effects of these features remain undetermined. The relict Chain and Charcot Fracture Zones have been shown to have controlled the stratigraphic architecture of the adjacent margins of Ghana and Ivory

Coast due to their proximity to these regions (de Matos, 2000). The relict Chain and Charcot Fracture Zones, as well as buried volcanoes (hotspots), have also been shown to play the role of buttressing or concentrating strain at the toe of the Niger Delta lobe (Davies *et al.,* 2005; Briggs *et al.,* 2009). For example, the Charcot Fracture Zone provides a prominent separation between the Eastern Niger Delta Lobe (ENDL) and Western Niger Delta Lobe (WNDL) (Fig. 1A, B), while faults above the Chain Fracture Zone have linked to strain localisation (Morgan, 2004; Cobbold *et al.,* 2009). In the WNDL, the Chain and Charcot Fracture Zones are oriented oblique/parallel to the modern continental slope (Fig. 1A, B), and serve as transfer zones and control the position of submarine channels (Krueger and Grant, 2011).

Gravity-driven deformation on passive margins is generally dominated by gravity gliding and gravity spreading (Dejong and Scholten, 1973; Ramberg, 1981; Schultz-Ela, 2001). Gravity gliding is defined as a rigid, downward movement of sediment along a basal slip surface (regional detachment), while gravity spreading is defined as the lateral extension and vertical contraction of a linked system, regardless of basal slope or coherence of the system (Schultz-Ela, 2001). Gravity-spreading has been identified as the main mechanism of deformation of the Niger Delta's sedimentary wedge (Rowan *et al.,* 2004; Cobbold *et al.,* 2009; Wiener *et al.,* 2010; Pee *et al.,* 2014; Wu *et al.,* 2015). However, the timing and kinematics of deformation remain poorly understood. Gravity-spreading of the WNDL is driven by the presence of seaward-dipping bathymetric surface and high sedimentation/progradation rate of deltaic sediments above overpressured marine shales (see review in Morley *et al.,* 2011; Fig. 1C). Rapid burial of sediments at ~4 km beneath overburden, and differential compaction at ~4 km deep, result to overpressure within the shales, facilitating gravity-driven deformation (Doust and Omatsola, 1990; Morgan, 2004; Briggs *et al.,* 2006; Wiener *et al.,* 2010; Fig. 1C).

Despite numerous studies of the offshore WNDL over the past decade, the interplay of delta dynamics and paleo-topography as controls on gravity-driven deformation over the entire Niger Delta since the Cretaceous remains poorly understood. This is investigated in this study with specific focus on the Pliocene and the Pleistocene stratigraphic architecture of the offshore WNDL (Fig. 1), which is compared with the well-documented ENDL.

2. Regional setting

The Niger Delta is located in the Gulf of Guinea on the equatorial Atlantic margin of West Africa (Fig. 1). The unique tectono-stratigraphic setting of the Niger Delta has attracted both the industry and the academic investigations over the past decades as a natural laboratory to study (i) regional/global climate dynamics; (ii) sea-level changes (iii); gravity-driven deformation; (iv) evolution of river catchments, and (v) their control on sediment supply, distribution and overall stratigraphic architecture of a large progradational delta on passive continental margin (Jermannaud *et al.,* 2010; Rouby *et al.,* 2011).

Recent studies by Chardon *et al.* (2016) and Grimaud *et al.* (2017), demonstrated that the modern Niger catchment developed during the late Eocene-early Oligocene (~34-29 Ma), following a regional magmatic upwelling of the northern part of the region. Chardon *et al.* (2016) and Grimaud *et al.* (2017), also showed that the magmatic upwelling, triggered the re-organisation of the Niger catchment, with an overall increase in sediment supply to the offshore Niger Delta.

Wiener *et al.* (2010), demonstrated that the Niger Delta's 'Oligocene-Tortonian extensional zone' is in the present-day onshore (Fig. 1B), but was in the offshore at the time of deposition. During the Tortonian (~9.3 Ma), an overall increase in sedimentation triggered the seaward progradation of passive margin slope, burial of the 'Oligocene-Tortonian extensional zone', and the development of the extensional zone seawards (Fig. 1B). An additional increase in sedimentation was also documented in the offshore Niger Delta between the early Pliocene (5.3 Ma), and the early Pleistocene (1.8 Ma) (now 2.6 Ma; Gibbard *et al.,* 2014) (Haack *et al.,* 2000; Robin *et al.,* 2011; Grimaud *et al.* 2017). The ENDL records progradation with an overall increase in sedimentation between ~4 Ma to ~2.5 Ma, and retrogradation with an overall decrease in sedimentation onwards to present-day. Jermannaud *et al.* (2010), attributed the overall reduction in sedimentation in the ENDL to: (i) a regional migration of delta lobe/switch of sediment fluxes from the ENDL to the WNDL or,

(ii) a climatic warming of west Africa/aridification of the Niger catchment, led to an overall decrease in sediment supply in the entire Niger Delta.

The lithostratigraphy of the Niger Delta comprises the contemporaneous Akata, Agbada and Benin formations (Avbovbo, 1978; Doust and Omatsola, 1990; Fig. 1D). The 3-4 km thick sediments of the Akata Formation comprise parallel-laminated marine muds/shales, which ranges between Paleocene-recent, and generally is considered as the principal source rock (Avabovbo, 1978; Hack *et al.,* 2000; Fig. 1D). The Akata Formation serves as the root of overpressure in the Niger Delta (Hack *et al.,* 2000; Fig. 1D). The 2-9 km thick, deltaic sediments of the Agbada Formation, ranges between the Eocene-recent, and serve as reservoir/source-seal (Avbovbo, 1978; Doust and Omatsola, 1990; Hack *et al.,* 2000; Fig. 1D). The 2 km thick, fluvial to upper coastal plain sediments of the Benin Formation ranges between the Miocene-recent (Avbovbo, 1978, Fig. 1D). Gravity-driven deformation of the Niger Delta's sedimentary wedge since the late Eocene, resulted in the development of three structural zones, namely: (i) an extensional zone, dominated by seaward- and landward-dipping, normal faults; (ii) a translational zone, dominated by thrust/shale-cored anticlines and shale-withdrawal intraslope basins, and (iii) a contractional zone, dominated by imbricated thrust sheets and associated folds (Doust and Omatsola, 1990; Cohen and McClay, 1996; Morgan, 2004; Fig. 1C). Regional seismic observations, and analogue and numerical models, show that the deformation of sediments in these structural zones is generally complicated by the presence of multiple detachments (Corredor *et al.,* 2005; Briggs *et al.,* 2006; Wiener *et al.,* 2010; Sapin *et al.,* 2012; Bellingham *et al.,* 2014; Peel *et al.,* 2014; Restrepo-Pace*,* 2018; Fig. 1C).

3. Dataset and methodology

3.1 Seismic and well data

We combined seismic reflection and well data to study the tectono-stratigraphic evolution of the offshore western Niger Delta from the Cretaceous to present. Seismic reflection data comprised 21 widely spaced 2D lines (6 strike lines and 15 dip lines), which cover an area of ~4,120 km^2 on the continental shelf (Fig. 1B). Among these lines, one 500-km long strike line extends throughout Niger

Delta lobes (see the red line labelled Fig. 6 in Fig. 1B). Others lines include 3 regional dip lines that extend beyond the continental shelf, with the longest (>200 km), reaching the abyssal plain (see the red lines labelled Figs. 3, 4/10B, and 5 in Fig. 1B). The seismic reflection data was processed as zero-phase source wavelet in the American reverse standard polarity such that an increase in acoustic impedance corresponds to a trough (black loop) in the wavelet, while a decrease in acoustic impedance is represented by a peak (white loop). They are characterised by a sampling interval of 4 milliseconds two-way-travel time (TWT), and vertical resolution, which ranges between 25-40 m.

We analysed a total of 20 wells (15 on the continental shelf and 5 on the continental slope; Fig. 1B; Table 1). The wells on the continental shelf were labelled Izaga shelf (IZSH 1 to IZSH 15) (Fig. 1B; Table 1). The wells on the slope that were previously labelled as FM-1 to FM-5 in (Chima *et al.*, 2019), were labelled in this study as FMSL 1 to FMSL 5 (SL for slope; Fig. 1B; Table 1), to distinguish them from the shelf wells. While FMSL 1 to FMSL 5 generally provide gamma ray, resistivity, neutron, density and sonic logs, only IZSH 1, 4, 7, 13 and 15, had gamma ray, resistivity, neutron, density, or sonic logs (Table 1). FMSL 1 to FMSL 5, and IZSH 1, 2, 4, 6, 7, 11, 14 and 15, also had checkshot data (Table 1). Biostratigraphic studies were also available for FMSL 1 to FMSL 4 wells (see Figs. 2, 7 and 8 in Chima *et al.,* 2019), and were used to date the entire Neogene, from the Burdigalian to Messinian, on the continental slope. The Pliocene and the Pleistocene sedimentary records generally lack biostratigrahic data. Out of the 15 wells on the continental shelf, only IZSH 1, 4, 7, 13 and 15, contain biostratigraphic data for the Messinian interval (Table 1). Also, out of the 8 seismic surfaces that were identified on the continental slope, (see Chima *et al.,* 2019; Fig. 1B), only 3 surfaces (the Serravallian, Tortonian and Messinian), could be correlated up-dip to the continental shelf. The inferred early Pliocene, early Pleistocene and middle Pleistocene seismic surfaces (see Fig. 10 in Chima *et al.*, 2020), were also correlated up-dip to the continental shelf. The age of an older seismic surface (the late Eocene), which was not penetrated by the wells that we studied, was estimated from Bellingham *et al.* (2014; Fig. 1C).

3.2 Methodology

3.2.1 Seismic stratigraphy

This study builds on the recently published sequence stratigraphic and cyclostratigraphic studies of the 3D seismic survey located on the western Niger Delta continental slope (see Figs. 5 and 10 in Chima *et al.,* 2019; 2020), respectively. These studies applied the sequence stratigraphic approach described by Mitchum and Vail (1977), which combines the recognition of amplitudes of seismic reflection, continuity, internal architecture, external geometry, nature of bounding surfaces, and erosional truncations. Seismic stratigraphy was calibrated with detailed 3D seismic geomorphological analysis to delineate key sequence stratigraphic surfaces (see Figs. 5, 10 and 12 in Chima et *al.,* 2019). Detailed analysis of calcareous nannofossil and planktonic foraminifera data from FMSL 1-4, were used to date stratigraphic surfaces from the Burdigalian to the Messinian (see Figs. 5, 7 and 8 in Chima *et al.,* 2019), for a more detailed explanation.

Despite the abundance of wells on the continental shelf (Fig. 1B; Table 1), their general lack of biostratigraphic data did not allow the direct calibration of the ages of the 5 stratigraphic surfaces identified in this region. However, this challenge was overcome by extending the 8 biostratigraphic and cyclostratigraphic surfaces (combined), identified on the continental slope (see Chima *et al* 2019; 2020), down-dip to the abyssal plain, and up-dip to the continental shelf. This was achieved with the aid of 6 interconnecting, regional 2D seismic lines (see the red lines in Fig. 1B). The general decrease in the vertical resolution of seismic data at depths >3.5 seconds two-way travel time (TWT), coupled with the abundance of growth faults and their associated shadow zones, locally hampered stratigraphic correlation notably in the outer shelf. However, signal processing algorithms in Petrel ™ software (median filter and structural smoothing), as well as reflection matching using 'ghost method', helped to improve the overall reflection continuity and aid seismic interpretation. Although we followed the conventional rules and meticulously interpreted our data, we are aware that the level of uncertainty in the correlation of stratigraphic surfaces across major growth faults, and laterally away, may be up to 50 m.

3.2.2 Velocity analysis, time-depth conversion and estimates of average sedimentation rates

After a detailed quality control of the checkshot data of five wells (FMSL 1-5; Fig. 1B, Table 1), we carried out the analysis of average velocity (m/s) vs, measured depth (m) on the deepest FMSL

1 well, which was drilled to a total depth of 4,154 m (see Figs. 2 and 7 in Chima *et al.,* 2019). We used the 'layer cake' approach in which we first defined stratigraphic units identified in the seismic data (Fig. 2). We plotted average velocity (V_{avg}) vs, measured depth (MD), and used a linear regression to define the relationship between velocity and depth for each stratigraphic unit (Fig. 2). The slope (K) and intercept (Vo) of this linear relationship (V=KZ+Vo) made it possible to build a time-to-depth conversion model. FMSL 1 well, only sampled the uppermost part of the late Eocene-Burdigalian Unit (Fig. 2). Therefore, we extrapolated the linear function using velocity-depth information estimated from a published line, a few kilometres from this study (see Bellingham *et al.,* 2014: Fig. 1B, C). This allowed us to obtain a consistent linear function down to the late Eocene surface (Fig. 2). We converted TWT surfaces to depth surfaces starting from the seafloor (the reference depth), using Petrel ™ software.

Due to the widely-spaced nature of the 2D seismic lines, estimates of average sediment thickness and average sedimentation rates were made on key regional seismic profiles (Fig. 1B). Average sedimentation rates were estimated on the seismic lines (labelled Figs. 4/10B and 5 in Fig. 1B). This was achieved by measuring the present-day surface area (km^2) of each key stratigraphic unit, defined as a faulted polygon (length and height in kilometers). This surface area was divided by the length (km) of the seismic lines to obtain the average sediment thickness (km) of each unit. This average sediment thickness was in turn divided by the duration of deposition (Ma) of the unit to obtain average sedimentation rates (km/Myr).

The main uncertainty in the above workflow (velocity model, estimates of average sediment thickness and depositional rates) is that it was entirely based on the deepest FMSL 1 well on the continental slope. This is due to the lack of wells in the deep basin, and the ones on the continental shelf have a limited penetration or lack checkshot data (Figs. 1B, C; 2; Table 1). Secondly, due to the lack of checkshot data within the first 1,378 m and below 4,050 m, velocity-depth plots in these intervals were based on extrapolation and information from a published study (see Bellingham *et al.,* 2014; Fig. 1B, C). The overall poor seismic reflectivity within the deeper stratigraphic intervals (e.g., the late Eocene-Serravallian), across major growth faults and imbricated thrusts, locally impacted seismic interpretation, estimates of average sediment thickness and depositional rates. Estimated average sediment thickness and depositional rates were based on selected, widely spaced 2D lines,

which do not represent the entire offshore WNDL. Regardless of the foregoing challenges and the overall shallowing of the stratigraphic surfaces above the Pleistocene, below the Burdigalian, and away from the continental slope, we obtained depth profiles, stratigraphic thicknesses and depositional rates that are comparable with published studies.

4. Results

4.1 Stratigraphic units

We extended the previously identified stratigraphic units from the continental slope (see Chima *et al.*, 2019 and 2020), up-dip to the continental shelf, and down-dip to the deep basin (see the red lines in Fig. 1B). The correlation of stratigraphic surfaces across regional, depth-penetrating 2D seismic lines (Fig. 1B), allowed us to investigate the control of delta dynamics and paleo-topography on gravity-driven deformation of the offshore WNDL since the Cretaceous (Figs. 3-6; 8).

4.1.1. The late Cretaceous-late Eocene Unit

4.1.1.1. Description: The late Cretaceous-late Eocene Unit is the oldest stratigraphic unit identified in the offshore WNDL (Figs. 3-5). It is bounded at the base and top by moderate-to high-amplitude seismic reflections (marked in dark green and light blue, respectively; Figs. 3, 4A, 5A). The Cretaceous and late Eocene ages, assigned to these seismic reflectors were based on comparison of our seismic lines (Figs. 3 and 4) with that of Bellingham *et al.* (2014; Fig. 1C). The late Cretaceous surface (labelled TB in Figs. 3-6), caps the underlying, acoustic seismic unit, marked by chaotic, moderate-to high-amplitude seismic reflections. This acoustic seismic unit is locally overlain in the

WNDL by a wedge-shaped, high-amplitude seismic reflections, highlighted in yellow in Fig. 6A, B. A moderate-to high-amplitude seismic reflector (labelled RD in Figs. 3, 4A, 5A), at the middle part of the late Cretaceous-late Eocene Unit, sub-divides the unit into 2 low- reflectivity sub-units (labelled LDU and UDU in Figs. 3-5). The LDU and UDU are highlighted in light and dark-grey, respectively (Figs. 4B, 5B). The late Cretaceous-late Eocene Unit generally decreases in thickness seaward, with its upper sub-unit, displaying remarkable thickness within the translational zone and the inner-fold-thrust belt (IFTB), where linear features, characterised by listric geometries are common (Figs. 3-5). The late Cretaceous-late Eocene Unit reaches an average thickness of 1.8 km and 2.1 km in Figs. 4 and 5, respectively. On a delta-wide strike line located on the continental shelf (Figs. 1A; 6), the late Eocene surface interpreted on the regional dip lines (Figs. 3-5), could not be identified due to seismic wipe-out (Fig. 6A). The poor reflectivity seismic unit (the interval highlighted in red in Fig. 6 B), displays a remarkable lateral variation in thickness, with an average of 1.2 km. The unit generally thins at the crests of paleo-structural highs in the central and western Niger Delta (Fig. 6A, B). Linear features that offset seismic reflections are distributed throughout the delta-wide strike line, and are poorly imaged within the deeper stratigraphic intervals (Fig. 6). On regional dip lines (Figs. 3-5), these linear features display high angles of inclination within the younger stratigraphy but develop listric geometry within the deeper stratigraphy. These linear features generally terminate at obliques angles on the regional seismic surface (labelled RD in Figs. 3-5). In map view, these linear features measure between 50-100 km in length, with parallel to sub-parallel geometry to the modern coastline (Fig. 1B). They range in dip orientation from dominantly landward in the ENDL to dominantly seaward, towards WNDL (Fig. 1B).

4.1.1.2. Interpretation: The seismic unit, characterised by chaotic, moderate-high amplitude reflectors, bounded at the top by a high-amplitude seismic reflector, is interpreted as the acoustic basement (Figs. 3-6). The paleo-structural highs identified in the central and western Niger Delta, are interpreted as the Charcot and Chain Fracture Zones, respectively (see Short and Stauble, 1967; Evamy *et al.,* 1978; Figs. 1A, B; 6A, B, D, E). The wedge-shaped, high-amplitude reflectors, which overlie the Chain Fracture Zone to the west, are interpreted as syn-rift deposits (Fig. 6A, E). The

lateral variation in thickness of the reflection-free seismic unit (highlighted in red in Fig. 6B), with an overall thinning at the crests of the Charcot and Chain Fracture Zones, indicate that these paleo-topographies exerted depositional control on the geometry of the unit. The reflection-free seismic units (labelled LDU and UDU in Figs. 3-5), which overlie the basement, are interpreted as lower and upper detachment units, respectively (see Bellingham *et al.,* 2014; Fig. 1C). The moderate to high-amplitude seismic reflector (labelled RD in Figs. 3-5), which delimits the lower and upper detachment units, is interpreted as a regional detachment/décollement (see also Bellingham *et al.,* 2014; Fig. 1C). This interpretation is supported by the termination of most linear features on this surface (Figs. 3-5). The normal and reverse offsets of seismic reflectors across linear features, support the presence of normal and thrust faults, respectively (Figs. 3-5). The bathymetric highs (labelled BH in Figs. 4 and 5), are interpreted as thrust/mobile shale-cored anticlines. The negative topographies that flank the thrust/shale-cored structures, are interpreted as intraslope basins (ISBs) (see also Adeogba *et al.,* 2005; Bakare *et al.,* 2007; Prather *et al.,* 2012., Chima *et al.,* 2019; 2020; Fig. 4B). The reflection-free interval (highlighted in red in Fig. 6B), where the late Eocene and the Burdigalian surfaces could not be tracked (Fig. 6A), suggests burial of sediment below the resolution of our seismic data. The overall thickening of the UDU within the translational zone and IFTB, is interpreted as structural thickening linked to duplexing (Figs. 4 and 5). Duplexing could also be responsible for the thickening of the LDU within the translational zone and IFTB (see also Jolly *et al.,* 2016; Fig. 4B).

4.1.2 The late Eocene-Serravallian Unit

4.1.2.1. Description: The late Eocene-Serravallian Unit is bounded at the base and top by undulating, moderate to high-amplitude seismic reflectors, highlighted in light blue and black in Figs. 3-5. This seismic reflector marks a transition from the underlying transparent unit to the overlying, moderate to high-amplitude seismic reflectors (Figs. 3-5). The unit is marked in the middle by an undulating seismic reflector, which was dated as Burdigalian by Chima *et al.* (2019) using biostratigraphic data (see the pink horizon in Figs. 3-5). The late Eocene-Serravallian Unit displays a total average thickness of 0.46 km, comprising 0.25 km for the late Eocene-Burdigalian, and 0.21 km for the

Burdigalian-Serravallian (Fig. 7A). The unit displays an overall uniform thickness within the extensional and contractional zones, but thickens within an intraslope basin, located seaward of the thrust fault (labelled T in Fig. 4D). The late Eocene-Serravallian Unit locally thins at the top of bathymetric highs formed by thrust/shale-cored anticlines (e.g., the thrust faults labelled T, U in Fig. 4D). The late Eocene-Serravallian Unit is locally truncated within the IFTB by the Tortonian surface (Fig. 4E).

4.1.2.2. Interpretation: The overall uniform thickness of the late Eocene-Serravallian Unit across the normal faults (labelled P-S and I-O in Figs. 3-5), suggests that the modern offshore western Niger Delta's extensional zone was not active during the late Eocene and the Serravallian. This interpretation supports the location of the 'Oligocene-Tortonian' extensional zone within fault-bounded accommodation in the present-day onshore (see Winer *et al.,* 2010; Fig. 1B). However, the seaward increase in thickness of the late Eocene-Serravallian Unit within the hanging wall of the thrust fault (labelled T in Fig. 4D), could be interpreted as growth strata associated with the activity of the thrust fault. Although this observation coupled with the corresponding thinning of the late Eocene-Serravallian Unit at the crest of thrusts/shale-cored anticlines (Fig. 4D), further supports that the underlying thrusts/duplexes were active during the deposition of the unit, similar stratigraphic architecture has also been linked to differential compaction by other authors (e.g., Maloney *et al.,* 2010). Similarly, the undulating geometry of the late Eocene, Burdigalian and Serravallian surfaces within intraslope basins (Figs. 3, 4A, B, D, E, and 5A, B), supports differential compaction or the activity of the underlying duplexes during the late Eocene-Serravallian. The abrupt truncation of the Burdigalian surface by the Serravallian surface in the IFTB (Fig. 4E), suggests that the activity of the underlying duplexes, caused local instability, allowing erosion/remobilisation at the crest of thrust/shale-cored anticlines, associated with the thrust faults (labelled V and W in Fig. 4E).

4.1.3. The Serravallian-Tortonian Unit (12.5-9.5 Ma).

4.1.3.1. Description: The Serravallian-Tortonian Unit is bounded at the base by the Serravallian surface described above and at the top by the Tortonian surface (highlighted in light green in Figs. 3-6). The Tortonian surface generally truncates seismic reflectors at the crest of thrust/shale-cored anticlines within the IFTB (Fig. 4E). Estimated average thickness of the Serravallian-Tortonian Unit is 0.24 km (Fig. 7A). The unit displays an overall constant thickness within the outer-fold-thrust belt (OFTB), but slightly thickens on the hanging walls of the normal faults (labelled S in Figs. 3; 4C, and I, J in Fig. 5A, B). The Serravallian-Tortonian Unit generally thins above thrusts/shale-cored anticlines within the translational zone and inner-fold-thrust belt (IFTB), but thickens within the adjacent intraslope basins (e.g., Fig. 4D, E). Along the 500-km, delta-wide strike line located on the continental shelf (Fig. 1B), the Serravallian-Tortonian Unit shows an overall constant thickness in the ENDL (Fig. 6C, D). The Serravallian-Tortonian Unit increases in thickness to the WNDL, and on the hanging walls of listric normal faults above the Chain Fracture Zone (Fig. 6E).

4.1.3.2. Interpretation: The truncation of seismic reflectors (e.g., the Burdigalian and Serravallian) by the Tortonian surface within the IFTB (Fig. 4E), suggests that the activity of the underlying duplexes caused instability, allowing erosion at the crest of thrust/shale-cored structures (e.g., Fig. 4E). The local thickening of the Serravallian-Tortonian Unit on the hanging walls of the normal faults (labelled S in Figs. 3, 4C and, I and J, in Fig. 5), is interpreted as growth strata, synchronous with the deposition of the unit. Similarly, the overall thickening of the Serravallian-Tortonian Unit within intraslope basins in the translational zone, and the corresponding thinning at the top of thrust/shale-cored anticlines (Fig. 4D, E), are interpreted as recording syn-depositional activity of the underlying thrusts/mobile shales. The along-strike variation in thickness of the unit, with an overall thickening from ENDL to WNDL is interpreted as recording differential subsidence/compaction, and changes in location of sediment input to the delta (see also Jermannaud *et al.,* 2010; Rouby *et al.,* 2011; Fig. 6B-E).

4.1.4. The Tortonian-early Pliocene Unit (9.5-4.9 Ma)

4.1.4.1. Description: The Tortonian-early Pliocene Unit is bounded at the base by the Tortonian surface described above, and at the top by the early Pliocene surface (highlighted in red in Figs. 3-6). The Tortonian and early Pliocene reflectors locally display undulating, concave-upward geometry, marked by abrupt truncations of the underlying reflectors, notably at the crest of thrust/shale-cored anticline within the extensional and translational zones, as well as the IFTB (Figs. 3 and 4D-E). The Tortonian-early Pliocene Unit reaches an average thickness of 0.25 km (Fig. 7A). It displays a lateral variation in thickness with local thickening on the hanging walls of the of the normal faults (labelled Q and S in Figs. 3, 4C, and I, J in Fig. 5B). The Tortonian-early Pliocene Unit generally thins above thrust/shale-cored anticlines (Figs. 3, 4D-F), but thickens within the adjacent intraslope basins (e.g., Fig. 4D, E). Along the delta-wide seismic line on the continental shelf (Fig. 1A), the Tortonian-early Pliocene displays a lateral variation in thickness with an overall increase from the eastern to western Niger Delta lobe (Fig. 6C-E).

4.1.4.2. Interpretation: The local truncations of reflectors below the Tortonian and early Pliocene surfaces suggest their erosional character, linked to the activity of the underlying thrusts (labelled T in Fig. 4D, V, W in Fig. 4E, and X in Fig. 4F). The reflectors truncated at the early Pliocene surface, seaward of the bathymetric high (labelled BH in Fig. 5B), is also linked to the activity of the underlying thrust. The overall thickening of the Tortonian-early Pliocene Unit across the hanging walls of the normal faults (labelled Q, S in Figs. 3, 4C, and I, J in Fig. 5B), is interpreted as growth strata. The along strike variation in thickness of the Tortonian-early Pliocene Unit, with an overall thickening from ENDL to WNDL, is interpreted as recording differential subsidence probably in response to changes in sediment loading (see also Jermannaud *et al.,* 2010; Rouby *et al.,* 2011; Fig. 6B-E). The general increase in thickness of the Tortonian-early Pliocene Unit, within intraslope basins, and the concomitant thinning at the crest of thrust/shale-cored anticlines (Figs. 4D, F; 5B), are interpreted as syn-depositional deformation (see also Maloney *et al.,* 2010). The relatively smooth geometry of the Tortonian-early Pliocene surfaces within the intraslope basin, seaward of the thrust

fault (labelled T, U in Fig. 4D), suggests that the underlying duplexes were not active during the deposition of the unit. However, the undulating geometry of the Tortonian-early Pliocene surfaces further west of the study area (Figs. 3 and 5B), suggests activity of the underlying thrusts. The erosional character of the early Pliocene surface in the extensional zone (Figs. 3 and 4C), translational zone and IFTB (Figs. 3; 4D, E), suggests the possible development of the surface during a relative sea-level fall and increase in sediment supply in the early Pliocene (see also Chima *et al.,*2019, 2020).

4.1.5. The early Pliocene-early Pleistocene Unit (4.9-5.0 to ~2.6 Ma)

4.1.5.1. Description: The early Pliocene-early Pleistocene Unit is bounded at the base and top by the seismic reflectors marked in red and dark yellow, respectively in (Figs. 3-6). The early Pliocene and early Pleistocene surfaces locally truncate seismic reflectors within the extensional and translational zones, as well as IFTB and OFTB (e.g., Figs. 3, 4C-F; 5B). The early Pliocene-early Pleistocene Unit reaches an average thickness of 0.23 km (Fig.7A). It is generally thicker on the hanging walls of the normal faults (labelled Q, P, S, in that order), on the shelf than in intraslope basins in the translational zone (Figs. 3, 4B-D; 5B). The early Pliocene-early Pleistocene Unit thickens within intraslope basins in the translational zone and IFTB, but thins above shale/thrust-cored anticlines, down to the OFTB, where it onlaps a basement high (labelled BH in Figs. 3, 4B, D, E, C, F; 5B). Within the early Pliocene-early Pleistocene Unit, seaward-inclined linear scars (hashed white lines in Fig. 4D, E), are locally present at the top of thrust/shale-cored anticlines, that are flanked by mass-transport deposits (MTDs) in the translational zone. On the delta-wide strike line on the continental shelf (Fig. 1A), the early Pliocene-early Pleistocene Unit shows a lateral variation in thickness with an overall thinning to the eastern and western edges of the delta. The early Pliocene-early Pleistocene Unit thickens towards the central part of the delta (Fig. 6B-E). The observed lateral variation in thickness along the delta-wide strike line is partially controlled by the alignment of the line with growth faults in the eastern, central and western part of the delta (Fig. 1A).

4.1.5.2. Interpretation: The truncations of reflectors by the early Pliocene surface on the continental shelf and slope (e.g., Figs. 3, 4C-E), suggests its erosional character, probably developed during a sea-

level fall in the early Pliocene (see also Chima *et al.,* 2020). The presence of seaward-dipping scars (interpreted as headwall scars) at the crest of thrust/shale-cored anticlines (Fig. 4D, E), suggests the role of thrusting in triggering mass-wasting. This interpretation is supported by the presence of MTDs within the adjacent intraslope basins (Fig. 4D, E). The general truncation of reflectors by the early Pliocene surface at the crest of thrust/shale-cored anticlines (e.g., Figs. 3; 4D, E, F; 5B), suggests syn-depositional activity of the structures. This interpretation is supported by the overall thinning of the early Pliocene-early Pleistocene Unit above thrust/shale-cored structures, and the concomitant thickening within intraslope basins (e.g., Figs. 3; 4D, E, F; 5B). The general thickening of the early Pliocene-early Pleistocene Unit on the continental shelf and the upper slope (Figs. 3; 4B-D, and 5 B), is interpreted to record syn-depositional deformation during the deposition of the unit. The onlapping of early Pliocene-early Pleistocene Unit on bathymetric highs in the translational and contractional zones (Figs. 3; 4D, E, F; 5B), indicates that gravity-driven deformation was accommodated down-dip by shortening/folding.

4.1.6. The early Pleistocene-present (~2.6-0 Ma)

4.1.6.1. Description. The early Pleistocene-present Unit is bounded at the base by the early Pleistocene surface, and capped by the seafloor (Figs. 3-6). The early Pleistocene-present Unit is marked in the middle by a downlap surface (yellow reflector in Figs. 3-6). This downlap surface corresponds to the erosional surface, dated on the continental slope as the middle Pleistocene transition (0.8-1.0 Ma) (see Figs. 3 and 10 in Chima *et al.,* 2020). The early Pleistocene surface locally truncates the upper part of the Pliocene sediments in the extensional and translational zones, and OFTB (Figs. 3; 4E, F). The early Pleistocene-present Unit locally displays seaward-inclined scarps at the crest of thrust/shale-cored anticlines, which are flanked by MTDs in the adjacent intraslope basins (Fig. 4D, E). The unit reaches a highest average thickness of 0.5 km (Fig. 7A). The early Pleistocene-present Unit reaches maximum thickness on the continental shelf and upper slope, but gradually thins seaward to the OFTB, where it onlaps bathymetric highs (Figs. 3; 4B-F; and 5B).

Along the delta-wide strike line displayed in Figure 6A-B, the early Pleistocene-present Unit generally decreases in thickness from the eastern to the western Niger Delta lobe (Fig. 6A-E).

4.1.6.2. Interpretation: The truncation of seismic reflectors on the continental shelf by the early Pleistocene surface (e.g., Fig. 3), suggests its erosional character. This interpretation is supported by the erosional truncations of reflectors below the early Pleistocene surface in the IFTB and OFTB (Fig. 4E, F). The presence of headwall scarps at the crest of thrust/shale-cored anticlines (Fig. 4D, E), further supports the role of thrusting at steepening the slope and increasing its instability, allowing mass-wasting on the continental slope. The truncation of reflectors at the crest of thrust/shale-cored anticlines (e.g., Figs. 3; 4D, E, F), suggests the activity of the structures during the Pleistocene. The overall thickening of the early Pleistocene-present Unit within the hanging walls of normal faults in the extensional and translational zones is interpreted to record syn-depositional deformation (Figs. 3-6). However, the overall thinning/onlapping of the unit within the deep basin (Figs. 3-5), suggests that gravity collapse of the continental shelf and upper slope facilitated the creation of accommodation for sediment sequestration. The increase in thickness of the early Pleistocene-present Unit to the eastern Niger Delta lobe (Fig. 6A, B), suggests an overall increase flexural subsidence, linked to increase in sediment loading and/or gravity collapse of the eastern Niger Delta continental shelf.

4.2 Sedimentation rate

Estimated average sedimentation rates on key 2D seismic lines in the offshore WNDL (Fig. 7B) show relatively low depositional rates from late Eocene to Burdigalian. Average sedimentation rates range between 0.01 and 0.03 km/Myr, respectively during the late Eocene-Serravallian, to 0.08 and 0.16 km/Myr over the Serravallian-Tortonian. Sedimentation rates thus display at least a two-fold increase from the Burdigalian to the Tortonian. They gradually decrease by one third from the Tortonian to early Pliocene, and finally doubled from the early Pliocene to present (Fig. 7B), reaching respective peaks of 0.20 and 0.25 km/Myr at present-day.

5. Discussion

Regional depth-penetrating 2D seismic reflection data and calibration with well information allow us to discuss the tectono-stratigraphic evolution of the offshore western Niger Delta. We focus on the control of delta dynamics and paleo-topography on gravity-driven deformation of the delta from the Cretaceous to present. We also compare the stratigraphic architecture of the offshore WNDL with the ENDL over the Pliocene and Pleistocene.

5.1. Tectono-stratigraphic evolution of the offshore WNDL from the Cretaceous to present

The overall thinning of the late Eocene-Serravallian at the crest of the thrust/shale-cored anticline, and its thickening within the intraslope basin, seaward of the thrust fault (labelled T in Fig. 4 D), suggest syn-depositional deformation. This interpretation is supported by the undulating geometry of the late Eocene, Burdigalian and the Serravallian surfaces, interpreted as recording the activity of the underlying duplexes (Figs. 3, 4B, D; 5B). Magmatic upwelling and catchment reorganisation around ~34-29 Ma, as well as an increase in sediment supply in the offshore Niger Delta, reported by Chardon *et al.* (2016) and Grimaud *et al.* (2017), is thought to have triggered deformation of the late Eocene-Serravallian Unit. However, the overall uniform thickness of the late Eocene-Serravallian Unit within the extensional zone (Figs. 3-5), suggests that the depocenter was probably confined in fault-bounded accommodation in the present-day onshore (Fig. 1B). This interpretation agrees with previous studies of the ENDL, where deposition is reported to have been focused in the current onshore part [the 'Oligocene-Tortonian extensional zone' (see Billotti and Shaw, 2005; Wiener *et al.,* 2010)].

During the Serravallian and the Tortonian, the presence of growth strata on the hanging walls of the normal faults (labelled S in Figs. 3; 4C; I and J in Fig. 5A, B), suggests the onset of deformation within the currently active extensional zone. The overall thinning of the Serravallian-Tortonian Unit at the crest of thrust/mobile shale-cored anticlines, and its concomitant thickening within intraslope basins (Figs. 3-5), suggest that deformation within the extensional zone was accommodated by shortening/folding within the translational and contractional zones. The coupling

between extensional deformation and shortening suggests the onset of sediment bypass from depocenter fill in the 'Oligocene-Tortonian extensional zone' (the present-day onshore; Fig. 1B).

During the Tortonian-early Pliocene, the presence of growth strata from the extensional to contractional zones (e.g., Figs. 3; 4C-F; 5B), is interpreted to record regional, syn-depositional deformation. This regional deformation could be linked to the onset of seaward migration of the 'Oligocene-Tortonian extensional zone' from the present-day onshore to the modern continental shelf (see Billotti and Shaw, 2005; Wiener *et al.*, 2010; Fig. 1B). In the ENDL, the migration of the 'Oligocene-Tortonian extensional zone' from the onshore to its present-day position (Fig. 1B), was linked to an overall increase in sedimentation during the Tortonian (see Billotti and Shaw, 2005; Wiener *et al.*, 2010). The relatively low sedimentation rate over the Tortonian-early Pliocene (Fig. 1B), could be linked to uncertainties in biostratigraphic dating, seismic interpretation or velocity modeling, used in time-to-depth conversion.

The general thickening of the early Pliocene-early Pleistocene Unit within the extensional zone (e.g., Figs. 3; 4B, C; 5B, 6D, E), suggests an overall increase in deposition on the offshore western Niger Delta's continental shelf. This agrees with the incisional character of the early Pliocene surface (e.g., Figs. 3; 4C-E). The thinning/onlapping of the early Pliocene-early Pleistocene Unit at the crest of thrust/shale-cored anticlines, and thickening of the unit within adjacent intraslope basins (e.g., Figs. 4D-E; 5B), suggests that extensional deformation was accommodated by shortening in the deep basin. Sediment loading on the continental shelf, aided by the presence of a structural barrier, formed by thrust/shale-cored anticline (e.g., Fig. 4), are inferred to have facilitated gravity-spreading (see review in Morley *et al.,* 2011). Gravity spreading is also inferred to have been triggered by the presence of a seaward dipping bathymetric surface (Schulz-Ella, 2000; Rowan *et al.,* 2004; Peel *et al.,* 2014; Figs. 3; 4B; 5B). The onlapping of the early Pliocene-early Pleistocene Unit on a relief associated with the imbricated thrust (labelled Z in Fig. 4F), supports the initiation of the OTFB during the early Pliocene (see Wiener *et al.,* 2010).

The remarkable increase in sediment thickness over the early Pleistocene-present (Figs. 3-6), continued to drive gravity collapse/increase in accommodation, and gravity spreading of the offshore

WNDL. The onlapping of the early Pleistocene-present Unit on a bathymetric relief on the modern seafloor (Fig. 4F), indicates that the OFTB of the offshore WNDL was active in the Pleistocene, and may still be active.

We propose a five-stage schematic illustration of the tectono-stratigraphic evolution of the offshore WNDL from the late Cretaceous-present (Figs. 8, 9). A: Development of duplexes within the upper detachment unit; B: initiation of gravity-driven deformation within the currently active extensional and translational zones; C: coupling of deformation between the extensional, translational and contractional zones, and inferred migration of the 'Oligocene-Tortonian extensional zone' from the present-day onshore to the present-day continental shelf'; D: acceleration of gravity-collapse of the continental shelf, and initiation of the OFTB; E: intensification of gravity collapse and deformation at the leading front of the OFTB.

5.2 Controls of paleo-topography and delta dynamics on gravity-driven deformation of the offshore WNDL

The bathymetric highs formed by the Charcot and Chain Fracture Zones (Figs. 1A, B; 6A, B, D, E), acted as transform faults during the opening of the equatorial Atlantic in the middle Aptian (Lehner and de Ruiter, 1977; Briggs *et al.,* 2009). Although these relict transform faults are known to have been inactive in the Santonian (Lehner and de Ruiter, 1977; Briggs *et al.,* 2009), their relict topographies control the architecture of younger post-rift sediments. The relict Charcot and Chain Fracture Zones have been identified to have exerted a long-term depositional control (loading/differential compaction) on the architecture of Ghana and Ivory Coast in the west African margin (de Matos, 2000). The Chain Fracture Zones generally act as transfer zone for sediment partitioning to the deep basin (Krueger and Grant, 2011).

In this study, the general thinning of the late Cretaceous-Serravallian Unit at the crest of the relict Charcot and Chain Fracture Zones (Fig. 6A, B, D, E), suggests that the presence of these paleo-topographies exerted depositional control on the geometry of the unit. The thinning trend above these

paleo-topographies, and concomitant thickening on the flanks, support their role in buttressing or localising strain (see also Davies *et al.,* 2005; Briggs *et al.,* 2009; Figs. 1B; 6A-E). This interpretation is supported by the presence of listric, synthetic and antithetic faults, above the Charcot and Chain Fracture Zones (Fig. 6D, E). Although the Chain and Charcot Fracture Zones are generally interpreted as presently inactive, the concentration of listric and synthetic normal faults above these structures, support their role in strain localisation in addition to gravity-driven deformation and mechanical compaction. The observed higher sediment thickness at the flanks of the relict transform faults (Fig. 6A-F), have the potential of increasing regional overpressure within the detachment (Figs. 3-5). Also, differential subsidence on both sides of the relict transform faults is responsible for the segmentation of gravity-driven deformation in the eastern and western Niger Delta lobes (see Wu *et al.,* 2015). Although no evidence of re-activation of these paleo-transforms faults was observed in our data, their long-term control is visible on the architecture of the offshore WNDL (Fig. 6A-F).

5.3 Implication of sedimentation rates on the evolution of the offshore WNDL

In this study, the estimated average sedimentation rates on the offshore WNDL displays similar trend with Grimaud *et al.* (2017), with a relatively low depositional rates from the late Eocene to Burdigalian, and late Eocene to Langhian, respectively (Fig. 7B). The magmatic upwelling of the Hoggar Mountain and re-oganisation of the Niger catchment around ~34-29 Ma, are reported to have initiated an increase in sedimentation rate on the offshore Niger Delta (Chardon *et al.,* 2016; Grimaud *et al.,* 2017). However, the observed low sedimentation rate over the late Eocene-Burdigalian could be linked to (i) sediment trapping within the 'Oligocene-Tortonian extensional zone' (the present-day onshore; Fig. 1B), or (ii) compaction/porosity loss due to increase in burial depth. The overall increase in average sedimentation rate from the Burdigalian to Tortonian (Fig. 7B), is consistent with Grimaud *et al.* (2017). The increase in sediment supply is probably linked to a combination of sustained erosion of the Hoggar region (see Grimaud *et al.,* 2017), and/or intensification of sediment cannibalisation on the continental shelf as documented in other continental margins (see Séranne and

Nzé Abeigne,1999; Anka *et al.,* 2009; Grimaud *et al.,* 2017). The incision of the Niger Delta's continental shelf during the Miocene was first reported by the presence of clay-filled, Opuama channel complex (see Doust and Omasola; 1990; Fig. 1D). Grimaud *et al.* (2017), reported a general high sedimentation rate over the Tortonian-early Pliocene (Fig. 7B). However, the relatively low average sedimentation rate that we estimated during the Tortonian-early Pliocene (Fig. 7B), could be linked to (i) sediment trapping within the Niger catchment and/or (ii) sediment routing from west to east (Fig. 1B). The slight decrease in average sedimentation rate in the offshore WNDL during the Tortonian (Fig. 7B) differs from the overall increase reported in the ENDL by (Wiener *et al.,* 2010; Jolly *et al.,* 2016). Like Rouby *et al.* (2011), and Grimaud *et al.* (2017), our estimated average sedimentation over the Pliocene-Pleistocene, displays a (more than) two-fold increase (Fig. 7B). Earlier studies by Wiener *et al*. (2010); Robin *et al.* (2011); Rouby *et al.* (2011); Chardon *et al.,* (2016), and Grimaud *et al.,* (2017), linked the increase in sediment supply to the offshore Niger Delta over the Pliocene-Pleistocene to climatically-forced precipitation. Chima *et al*. (2020), suggested that glacio-eustatic sea-level oscillation of 400-kyr eccentricity, and intensification of West African Tropical Monsoon, could explain the general increase in sedimentation rate on the offshore WNDL during the Pliocene-Pleistocene.

Contrary to Rouby *et al.* (2011) and Grimaud *et al.* (2017), who documented a general decrease in sedimentation rate from the Pleistocene to present, our results show an overall increase in sedimentation rates (Fig. 7B). Although Grimaud *et al.* (2017), linked their estimated low sedimentation rate in the offshore WNDL during the Pleistocene to sediment trapping within the Niger catchment, their lack of data in the distal offshore could also explain their low interpreted depositional rates. Rouby *et al.* (2011) linked their observed reduction in sedimentation rate in the offshore ENDL from the Pleistocene to present to aridification of West Africa or a possible transfer of sediment flux from the ENDL to WNDL. The high sedimentation rates observed in this study from the Pleistocene to present is consistent with sediment budgets in other worldwide passive continental margins e.g., the offshore Alaska (Gulick *et al.,* 2015); the Alpine region (Molnar and England, 1990; Hay, 1998; Willett, 2010, Leroux et al., 2017). In these regions, the increase in sedimentation rate during most of the Pleistocene (Fig. 7B), is attributed to glacio-eustatic sea-level changes of 100-kyr

eccentricity, and intensification of the West African Tropical Monsoon at the middle Pleistocene Transition (MPT, ~0.8-1.0 Ma) (see also Chima *et al.,* 2020).

5.4 The Pliocene and Pleistocene stratigraphic architecture; eastern vs western Niger Delta lobes

Comparison of regional dip lines from the eastern and western Niger Delta lobes over the Pliocene and the Pleistocene, reveals that variation in structural patterns in these regions, controlled their stratigraphic architecture (Fig. 10A, B). The ENDL displays an overall higher slope angle compared to the WNDL (Fig. 10A, B). The higher shelf-slope angle of the ENDL compared to the WNDL, could be linked to the presence of seamount or buried volcanoes (e.g., de Matos, 2000; Mourges *et al.,* 2009). This interpretation is supported by the proximity of the seismic line (Fig. 10A) to the Fernando Po Fracture Zone (Fig. 1A, B).

Although the continental shelves of the ENDL and WNDL are characterised by seaward-and landward-dipping normal faults, they display overall progradation during the late Pliocene and the early Pliocene, respectively (Fig. 10A, B). The presence of well-developed counter-regional normal faults at the shelf-slope break of the ENDL, favored aggradation and sediment sequestration on the continental shelf and slope regions from the Pleistocene to present (Fig. 10A). However, the dominance of well-developed seaward-dipping normal faults in the WNDL, favoured an overall progradation and sediment bypass to the deep basin from the Pleistocene to present (Fig. 10B). We propose 2 possible explanations for the dominance of counter-regional normal faults on the continental shelf of the ENDL; (i) the relief formed by the Fernando Po Fracture Zone or buried volcanoes, thereby localising strain, or (ii) the presence of buried thrust faults (see also Sapin *et al.,* 2012).

We lack sufficient seismic and well data for complete source-to-sink mapping and estimation of sedimentation rates for a robust quantitative comparison between ENDL and WNDL. However, the observed geometries (Fig. 10A, B), clearly demonstrate that differences in gravity-driven deformation

in these regions, significantly controlled their evolution in a similar way during the Pliocene but differently during the Pleistocene.

6. Conclusions

(1) Limited sedimentary wedge deformation within the extensional and translational zones, offshore western Niger Delta lobe, from the late Eocene to Serravallian, suggests that the 'Oligocene-Tortonian extensional zone' is buried under the present-day onshore area. Regional distribution of deformation from the extensional zone to the transitional detachment fold-belt during the Tortonian, suggests seaward progradation.

(2) An overall increase in sedimentation on the continental shelf, offshore WNDL since the Serravallian, characterised by deformation within the extensional and translational zones, is thought to have triggered gravity-driven deformation. The increase in sedimentation in the Pliocene and Pleistocene, differential subsidence of the continental shelf and slope, and the presence of seaward-dipping bathymetry, aided the acceleration of gravity spreading. The increase in sedimentation rates during the Pliocene-Pleistocene, coupled with the presence of bathymetric relief on the modern seafloor, at the leading front of the contractional zone, supports the development of the present-day outer-fold-thrust belt in the Pliocene.

(3) Paleo-topographies formed by the Charcot and Chain Fracture Zones, which developed during the opening of the equatorial Atlantic, exerted depositional control on the stratigraphic architecture of the offshore WNDL from the Cretaceous to Serravallian. High sedimentation rates and differential subsidence across the relict Chain and Charcot Fracture Zones segmented gravity-driven deformation in the eastern and western Niger Delta lobes.

(4) The eastern and western Niger Delta lobes display an overall progradation and sediment bypass to the deep basin during the Pliocene. However, overall WNDL progradation continued during the Pleistocene, while the ENDL retrograded due to sediment sequestration on the continental shelf and upper slope. The ENDL and WNDL display complex spatial and temporal variations in

gravity-driven deformation, and sediment partitioning, during the Pliocene and the Pleistocene. Hence, more regional seismic and well data are needed for a more complete source-to-sink analysis of the systems.

(5) We propose a five-stage evolution of the offshore WNDL from the late Cretaceous-present

References

Adeogba, A.A., McHargue, T.R., & Graham, S.A. (2005). Transient fan architecture and depositional controls from near-surface 3D seismic data, Niger Delta continental slope. AAPG Bulletin 89, 627–643.

Anka, Z., Séranne, M., Lopez, M., Scheck-Wenderoth, M. & Savoye, B. (2009), The long-term evolution of the Congo deep-sea fan: a basin-wide view of the interaction between a giant submarine fan and a mature passive margin (ZaiAngo project). Tectonophysics, 470, 42-56.

Avbovbo, A. A., (1978). Tertiary lithostratigraphy of the Niger Delta: AAPG Bulletin, 62, 295–300.

Bakare, O., Hurley, N., & McHargue, T. (2007). Effect of Growing Structures on Stratigraphic Evolution, Channel Architecture, and Submarine Fan Distribution, Niger Delta, West Africa. AAPG Conference Proceedings, California.

Bellingham, P., Connors, C., Haworth, R., Barbara, R., & Danforth, Al. (2014). The deep-water Niger delta: an underexplored world class petroleum province. Petrol. Geosci. Mag. 11, 1–9.

Bilotti, F. D., Shaw, J. H., Cupich, R.M., & Lakings, R.M., (2005). Detachment fold, Niger Delta, in J. H. Shaw, C. Connors, and J. Suppe, eds., Seismic interpretation of contractional fault related folds: AAPG Studies in Geology 53, 103-104.

Briggs, S. E., Davies, R. J., Cartwright, J. A., & Morgan, R., (2006). Multiple detachment levels and their control on fold styles in the compressional domain of the deep-water west Niger Delta. Basin Research 18, 435–450. doi: 10.1111/j.1365-2117.2006. 00300.x.

Briggs, S. E., Cartwright, J., & Davies, R., (2009). Crustal structure of the deepwater west Niger Delta passive margin from the interpretation of seismic reflection data. Marine and Petroleum Geology 26, 936-950.

Chardon, D., Grimaud, J.-L., Rouby, D., Beauvais, A., & Christophoul, F. (2016). Stabilization of large drainage basins over geological time scales: Cenozoic West Africa, hot spot swell growth, and the Niger River: hot spot swell growth and Niger River. Geochemistry, Geophysics, Geosystems 17, 1164-1181.

Chima, K. I., Gorini, C, Rabineau, M., Granjeon, D., Do Couto, D., Leroux, E., & Hoggmascall, N., (2020). Pliocene and Pleistocene stratigraphic evolution of the western Niger Delta intraslope basins: A record of glacio-eustatic sea-level and basin tectonic forcings. *Global and Planetary Change. doi:* https://doi.org/10.1016/j.gloplacha.2020.103355

Chima, K. I., Do Couto D., Leroux, E., Gardin, S., Hoggmasacall, N., Rabineau, M., Granjean, D., & Gorini, C., (2019). Seismic stratigraphy and depositional architecture of Neogene intraslope basins, offshore western Niger Delta. Marine and Petroleum Geology 109, 449-468. *doi* https://doi.org/10.1016/j.marpetgeo.2019.06.030

Cobbold, P.R., Mourgues, R., & Boyd, K. (2004). Mechanism of thin-skinned detachment in the Amazon Fan: assessing the importance of fluid overpressure and hydrocarbon generation. Mar. Pet. Geol. 21, 1013–1025.

Cohen, H.A., & McClay, K. (1996). Sedimentation and shale tectonics of the northwestern

Niger Delta front. Marine and Petroleum Geology 13, 313-328.

Corredor, F., Shaw, J.H., & Bilotti, F. (2005). Structural styles in the deep-water fold and thrust belts of the Niger Delta. AAPG Bulletin 89, 753780. doi.org/10.1306/02170504074

Damuth, J. E., (1994). Neogene gravity tectonics and depositional processes on the deep Niger Delta continental margin: Marine and Petroleum Geology, 11, 320–346.

Davies, R.J., MacLeod, C.J., Morgan, R., & Briggs, S.E. (2005). Termination of a fossil continent-ocean fracture zone imaged with three-dimensional seismic data: the Chain Fracture Zone, eastern Equatorial Atlantic. Geology 33 (8), 641–644.

Dejong, K.A., & Scholten, R., (1973). Gravity and Tectonics. John Wiley, New York. 502.

Doust, H., & Omatsola, E. (1990). Niger Delta, in J. D. Edwards and P. A. Santogrossi, (Eds.); Divergent passive margin basins. AAPG Bulletin 48, 239-248.

Evamy, B.D., Haremboure, J., Kammerling, R., Knaap, W.A., Molloy, F.A., & Rowlands, P.H. (1978). Hydrocarbon habitat of Tertiary Niger Delta. AAPG Bulletin 62, 1-39.

Gibbard, P. L., Head, M.J., & Walker, M.J. (2014). Subcomission on stratigraphy Formal ratification of the Quaternary System/Period and Pleistocene Series/Epoch with a base at 2.5 Ma. Quaternary Science 245, 96-102.

Goudie, A. S. (2005). The drainage of Africa since the Cretaceous. Gemorphology (3-4), 437-456.

Grimaud, J.-L., Rouby, D., Chardon, D., & Beauvais, A. (2017). Cenozoic sediment budget of West Africa and the Niger delta. Basin Research, 1-18.

Gulick, S.P., Jaeger, J.M., Mix, A.C., Asahi, H., Bahlburg, H., Belanger, C.L., Berbel, G.B.,

Childress, L., Cowan, E., Drab, L. & Forwick, M. (2015). Mid-Pleistocene climate transition drives net mass loss from rapidly uplifting St. Elias Mountains, Alaska. Proc.Natl. Acad. Sci. Unit. States Am. 112, 15042–15047.

Haack, R. C., Sundararaman, P., Diedjonmahor, J.O., Hongbin, X, Gant, N.J., May, E. D., & Kelsch, K. (2000). Niger Delta Petroleum Systems, Nigeria. In: M.R. Mello and B.J. Katz, eds., Petroleum Systems of South Atlantic margins: AAPG Memoir 73, 213-231.

Hay, W.W. (1998). Detrital sediment fluxes from continents to oceans. Chemical Geology 145, 287-323.

Jermannaud, P., Rouby, D., Robin, C., Nalpas, T., Guillocheau, F., & Raillard, S. (2010). Plio-Pleistocene sequence stratigraphic architecture of the eastern Niger Delta: A record of eustasy and aridification of Africa. Marine and Petroleum Geology 27, 810-821.

Jolly, B.A., Lonergan, L., & Whittaker, A.C. (2016). Growth history of fault-related folds and interaction with seabed channels in the toe-thrust region of the deep-water Niger Delta. Mar. Pet. Geol. 70, 58–76.

Krueger, S.W., Grant, N.T. (2011). The growth history of the toe thrusts of the Niger Delta and the role of pore pressure. In: McClay, K.R., Shaw, J.H., Suppe, J. (Eds.), AAPG Memoir 94, Thrust fault-related Folding, 357-390.

Lehner, P., & de Ruiter, P.A.C (1997). Structural history of Atlantic margin of Africa. AAPG Bull. 61 (7), 961-981.

Maloney, D., Davies, R., Imber, J., Higgins, S., & King., S., (2010). New insights into deformation mechanisms in the gravitationally driven Niger Delta deep-water fold and thrust belt. AAPG Bulletin 94, (9), 1401-1424.

de Matos, R.M.D. (2000). Tectonic evolution of the equatorial Atlantic. Geophysical Monograph 115, 331-354.

Mitchum, R.M., & Vail, P.R., (1977). Seismic Stratigraphy and Global Changes of Sea Level, Part 7: Seismic Stratigraphic Interpretation Procedure: Seismic Stratigraphy: Applications to Hydrocarbon Exploration. AAPG Memoir 26, 135-143.

Molnar, P., & England, P. (1990). Late Cenozoic uplift of mountain and global climate change: chicken or egg? Nature 343, 29-34.

Morgan, R. (2004). Structural controls on the positioning of submarine channels on the lower slopes of the Niger Delta, in: Davies, R.J., Cartwright, J., Stewart, S.A., Underhill, J.R., Lappin, M. (Eds.), 3D Seismic Technology: Application to the Exploration of Sedimentary Basins. Geological Society of London Memoir 29, 45-51

Morley, C. K., King, R., Hillis, R., Tingay, M., & Backe, G. (2011). Deep-water fold and thrust belt classification, tectonics, structure and hydrocarbon prospectivity. Earth Sciences Reviews 104, 41-91.

Peel, F. J. (2014). The engines of gravity-driven movement on passive margins: Quantifying the relative contribution of spreading vs. gravity sliding mechanisms. Tectonophysics 633, 126-142.

Prather, B.E., Pirmez, C., Sylvester, Z., & Prather, D. S. (2012). Stratigraphic Response to Evolving Geomorphology in a Submarine Apron Perched on the Upper Niger Delta Slope. SEPM 99, 145-161.

Ramberg, H. (1981). Gravity, deformation and the Earth's crust in theory, experiments and geological application (2nd Edition): London, Academic Press, 452.

Restrepo-Pace, P. (2018). Ductile v. Brittle'-Alternative structural interpretations for the Niger Delta. Geological Society of London Special Publication 46, 1-12.

Robin, C., F. Guillocheau, S. Jeanne, F. P., & Calve`s, G. (2011). Cenozoic siliciclastic fluxes evolution around Africa, Geophys. Res. Abstr., 13, EGU, 2011-5659.

Rouby, D., Nalpas, T., Jermannaud, P., Robin, C., Guillocheau, F., & Raillard, S. (2011). Gravity driven deformation controlled by the migration of the delta front: The Plio-Pleistocene of the Eastern Niger Delta. Tectonophysics 513, 54-67. doi: https://doi.org/10.1130/GEOSO1426.1

Rowan, M. G., Peel, F. J., & Vendeville, B. C. (2004). Gravity-driven fold belts on passive margins: In: McClay, K. R. (Ed.), 2004. Thrust Tectonic and Hydrocarbon Systems, AAPG Memoir 82, 157-182.

Sapin, F., Ringenbach, J-C., Rives, T., & Pubellier, M. (2012). Counter-regional faults in shale-dominated deltas: origin, mechanism and evolution. Marine and Petroleum Geology 37, 121-128

Schultz-Ela, D. D. (2001). Excursus on gravity gliding and gravity spreading. Journal of Structural Geology, 23 (5), 725-731.

Séranne, M. & Nzé Abeigne, C. R. (1999) Oligocene to Holocene sediment drifts and bottom currents on the slope of Gabon continental margin (west Africa): consequences for sedimentation and southeast Atlantic upwelling. Sed. Geol., 128, 179-199

Short, K. C., & Stauble, A. J. (1967). Outline of geology of Niger Delta: AAPG Bulletin, 51, 761-779.

Sibuet, J.C., & Macle, J. (1978). Plate kinematic implications of Atlantic equatorial fracture zone trends. Journal of geophysical Research 83 (B7), 3401-3421.

Wiener, R.W., Mann, M. G., Angelich, M. T., and Molyneux, J. B., (2010). Mobile shale in the Niger Delta: Characteristics, structure, and evolution. AAPG, 93, 145-161.

Willett, S.C., (2010). Late Neogene Erosion of the Alps: A Climate Driver? Annual Review of Earth and Planetary Science 38: 37-411. doi: 10.1146/annurev-earth-040809-152543.

Wu, J. E., McClay, K., & Frankowicz, E. (2015). Niger Delta gravity-driven deformation above the relict Chain and Charcot fracture zones, Gulf of Guinea: Insights from analogue models. Marine and Petroleum Geology 65, 43-62.

Table 1. Summary of the seismic and borehole data used in this study.

Seismic	Type	Area (km^2)	Polarity	Phase	Frequency (Hz)	Sampling Interval (ms)	Vertical Resolution (m)
Shelf	2D	4,120	American	Zero	15-20	4	13.7-25
Slope	3D	638	reversed	phase	25-30	4	25-30
Well	GR	RES	NEU	DEN	DT	Checkshot	Biostratigraphy
IZSH 1	✓	✓	x	✓	✓	✓	✓
IZSH 2	✓	✓	x	✓	✓	✓	x
IZSH 3	✓	✓	x	✓	✓	x	x
IZSH 4	✓	✓	x	✓	✓	✓	x
IZSH 5	✓	✓	x	✓	✓	x	x
IZSH 6	✓	✓	x	✓	✓	✓	x
IZSH 7	✓	✓	x	x	✓	✓	✓
IZSH 8	✓	✓	x	x	x	x	x
IZSH 9	✓	✓	x	✓	✓	x	x
IZSH 10	✓	✓	x	✓	✓	x	x
IZHS 11	✓	✓	✓	✓	✓	✓	✓
IZSH 12	✓	✓	x	x	x	x	x
IZSH 13	✓	✓	x	✓	✓	✓	x
IZSH 14	✓	✓	x	✓	✓	✓	x
IZSH 15	✓	✓	x	✓	✓	✓	x
FMSL 1	✓	✓	✓	✓	✓	✓	✓
FMSL 2	✓	✓	✓	✓	✓	✓	✓
FMSL 3	✓	✓	✓	✓	✓	✓	✓
FMSL 4	✓	✓	✓	✓	✓	✓	✓
FMSL 5	✓	✓	✓	✓	✓	✓	x

GR-Gamma Ray; RES-Resistivity; NEU-Neutron; DEN-Density; DT-Sonic; Hz-Hertz; IZSH 1-15 and FMSL 1-5 stand for wells on the continental shelf and slope, respectively. See text for a more detailed explanation.

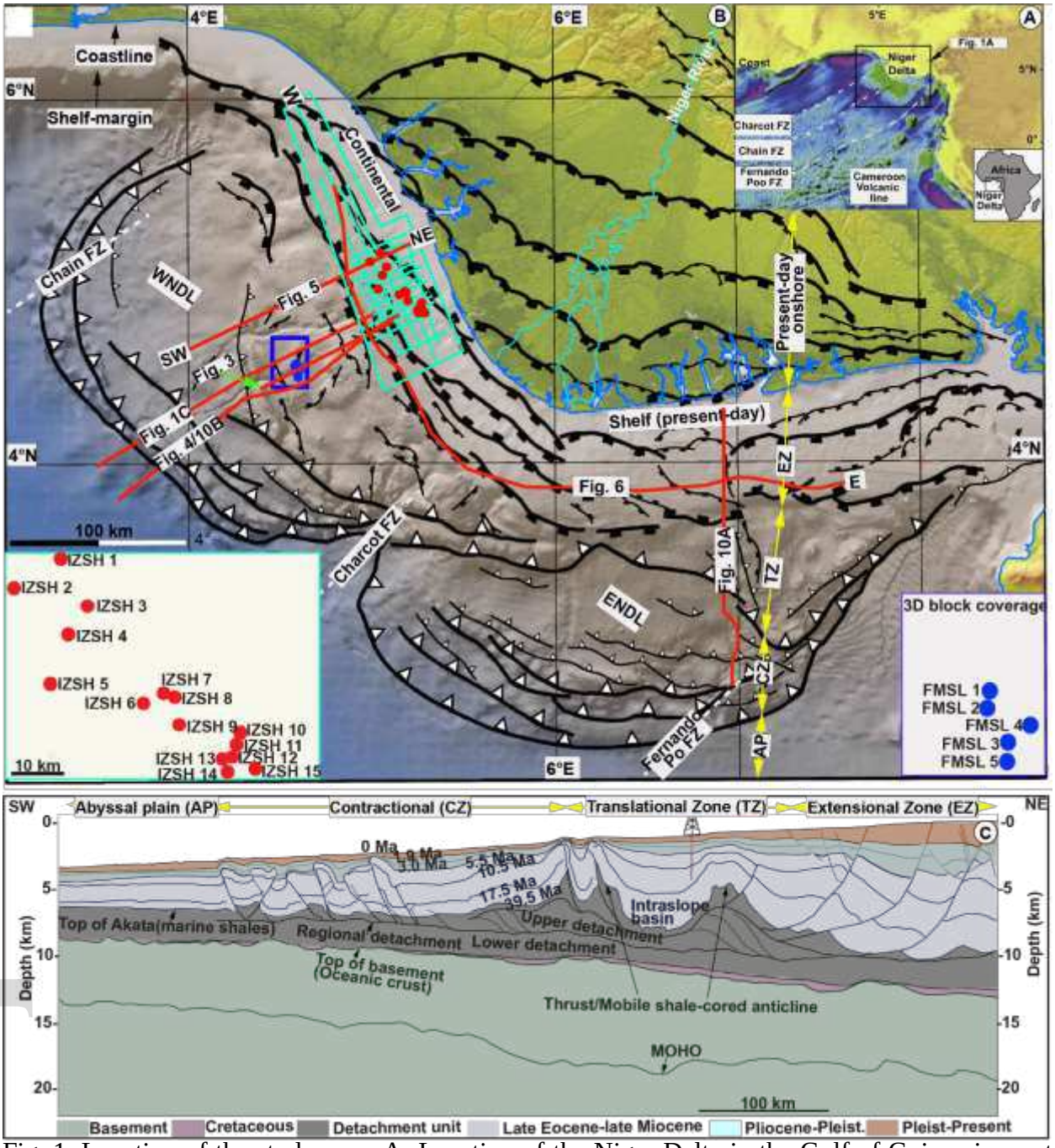

Fig. 1. Location of the study area. A: Location of the Niger Delta in the Gulf of Guinea in west Africa, offshore fracture zones and volcanic lines. B: Superposed relief and bathymetry map of the Niger Delta showing the extensional zone (EZ), translational zone (TZ), contractional zone (CZ) and the abyssal plain (AP) (modified after Rouby et al., 2011). The light green and red lines on panel B represent local and regional 2D seismic lines, respectively. Red circles show well locations

on the continental shelf (FMSL 1-5). The blue box and blue circles, show 3D seismic coverage, and well locations, respectively on the continental slope (IZSH 1-15). C: Regional line drawing, showing the structural styles of the offshore western Niger Delta (modified after Bellingham et al., 2014.

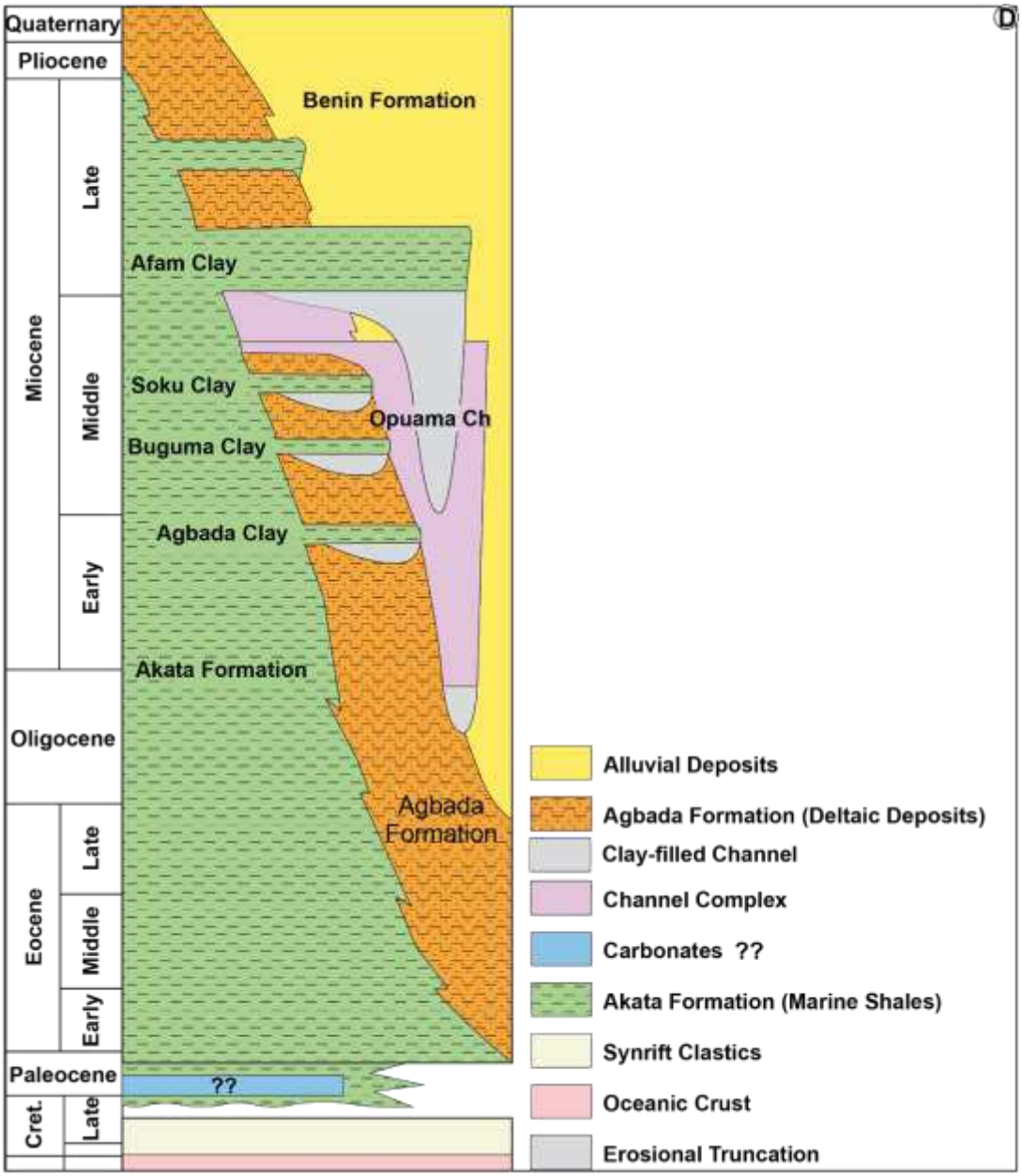

Fig. 1D. A schematic illustration of the lithostratigraphic units underlying the Niger Delta (modified after Corredor et al., 2005). See text for a more detailed explanation.

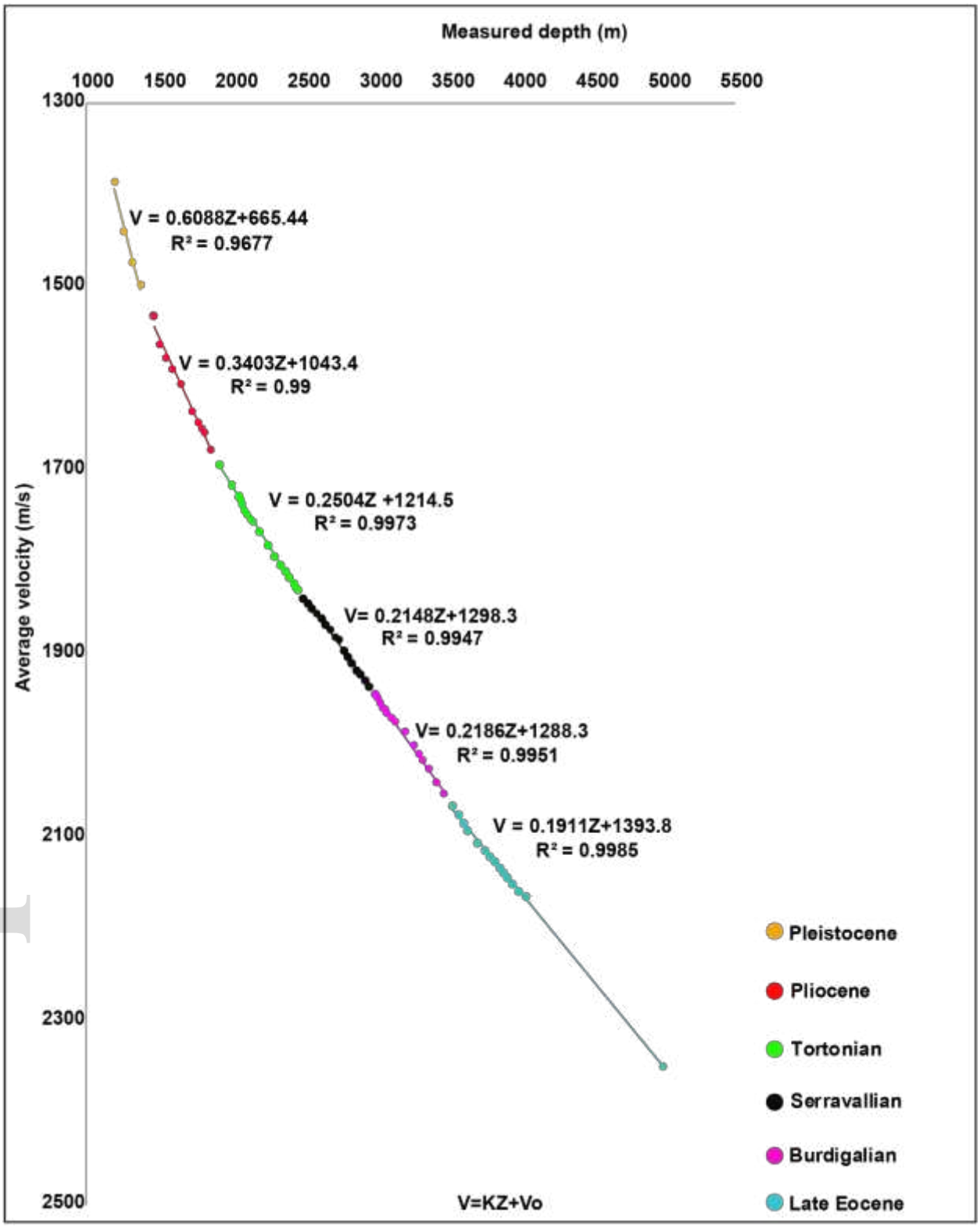

Fig. 2. Plot of average velocity (m/s) versus measured depth (m) extracted from the checkshot data of the deepest FMSL 1 well, used for depth conversion. See text for a more detailed explanation.

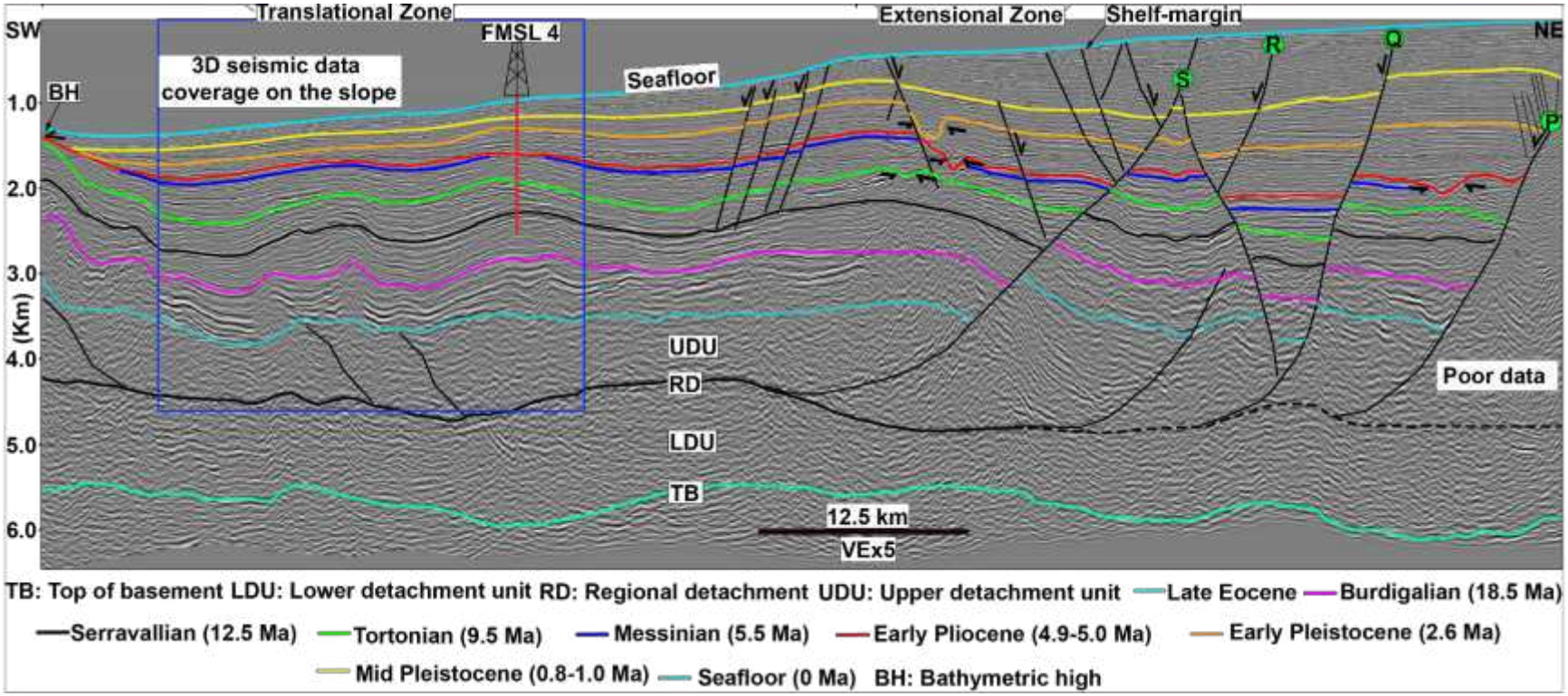

Fig. 3. Interpreted, regional seismic line (depth) (see Fig. 1B for location), showing the presence of landward-dipping top of basement (TB), and regional detachment (RD), underlain by lower detachment unit (LDU), and overlain by upper detachment unit (UDU). Note; (i) the listric geometry of normal faults, and their general termination on RD, (ii) undulating geometry of late Eocene to Tortonian surfaces, and (iii) a general increase in sediment thickness within the extensional zone from the early Pliocene to present. See text for a more detailed explanation.

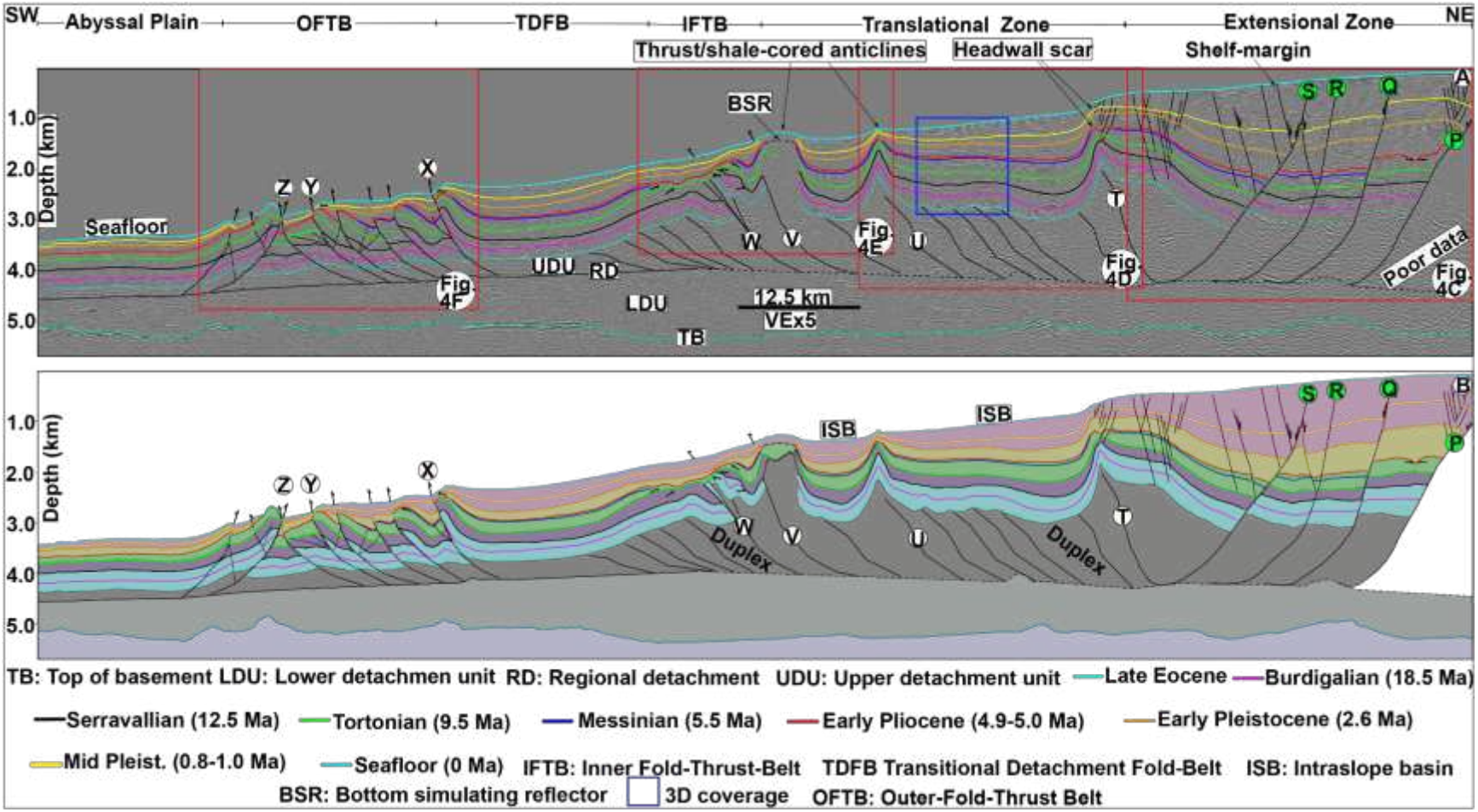

Fig. 4. A, B: Interpreted regional seismic line and line drawing (depth), showing the tectono-stratigraphic architecture of the offshore WNDL (see Fig. 1B for location). Note; (i) the listric geometry of normal faults within deeper stratigraphic intervals, and their general termination on RD, (ii) undulating geometry of late Eocene to Serravallian surfaces, and (iii) a general increase in sediment thickness

within the extensional zone from the early Pliocene to present. For more details, see zoomed sections outlined in red boxes in panel A (Fig. 4C-F).

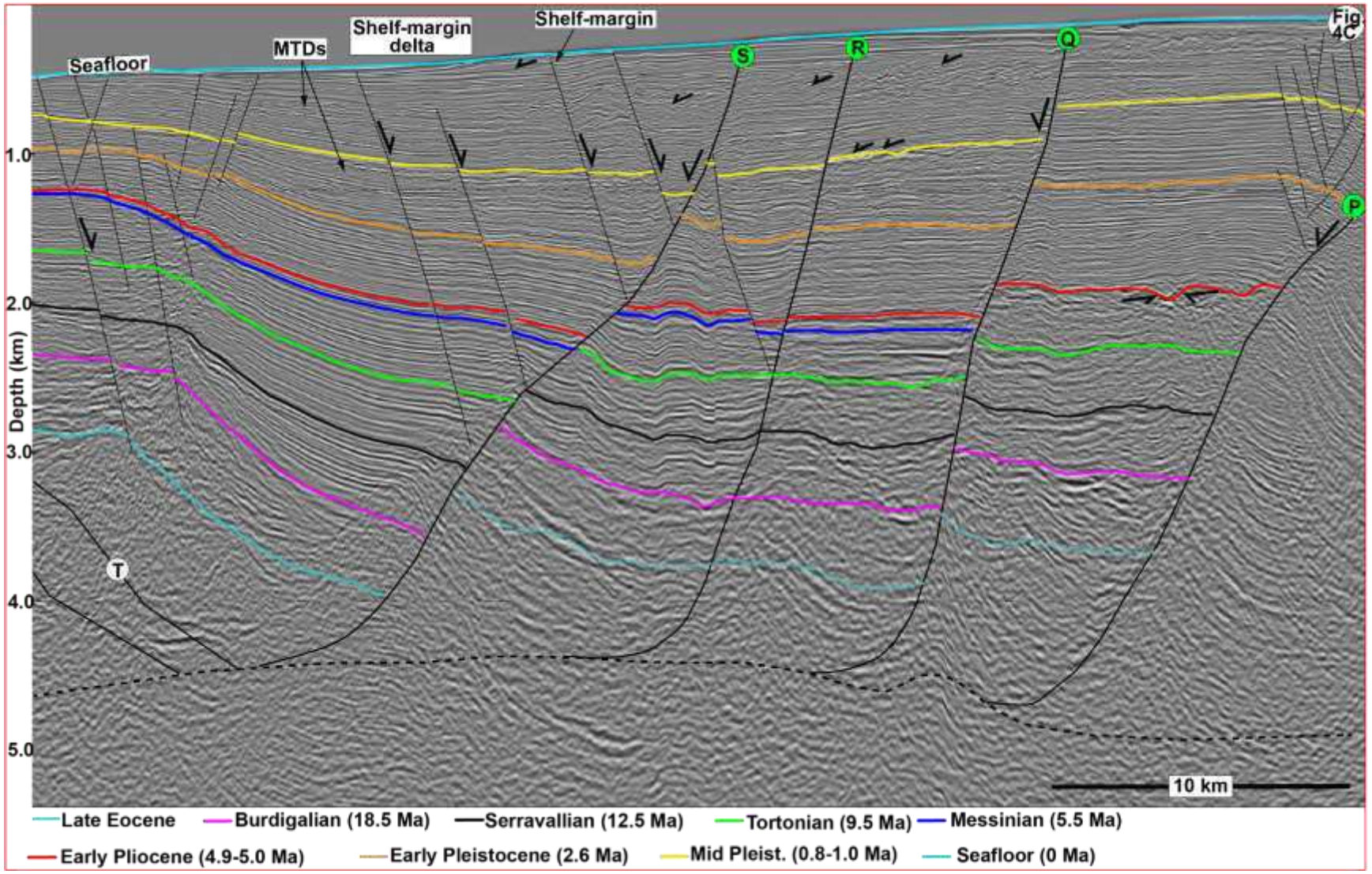

Fig. 4C. Detailed view of the extensional zone, showing the incisional character of the early Pliocene, and an overall thickening in stratigraphy.

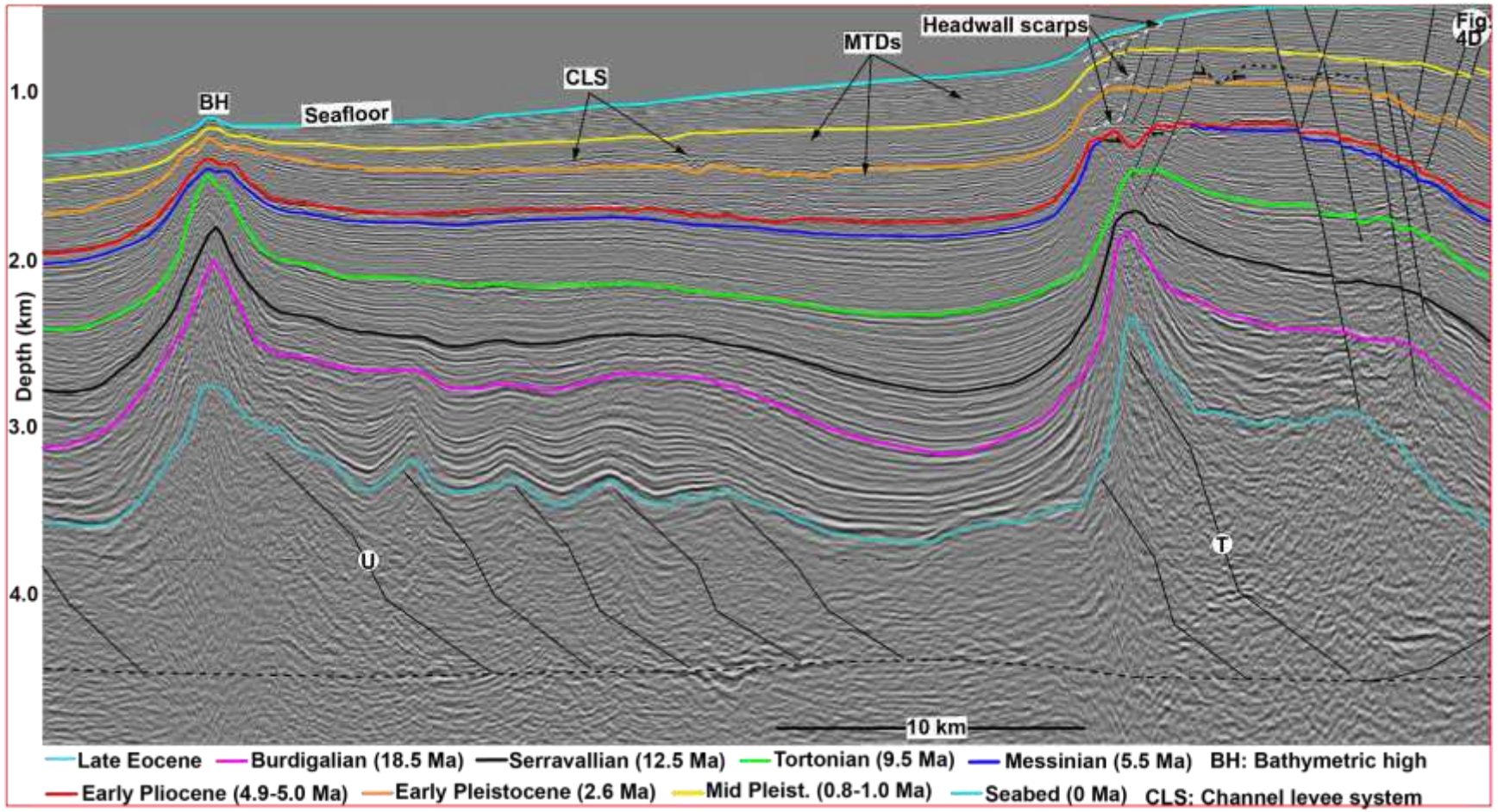

Fig. 4D. Detailed view of the translational zone, showing (i) the presence of BH (barrier), formred by thrust/shale-cored anticline, characterised by headwall scars at the shelf-slope break, (ii) an overall thinning of stratigraphy above BH, and concomittant thickening

within adjacent piggyback basin, (iii) incisional character of the early Pliocene surface, and (iv) undulating geometry of the late Eocene-Serravallian surface below duplexes.

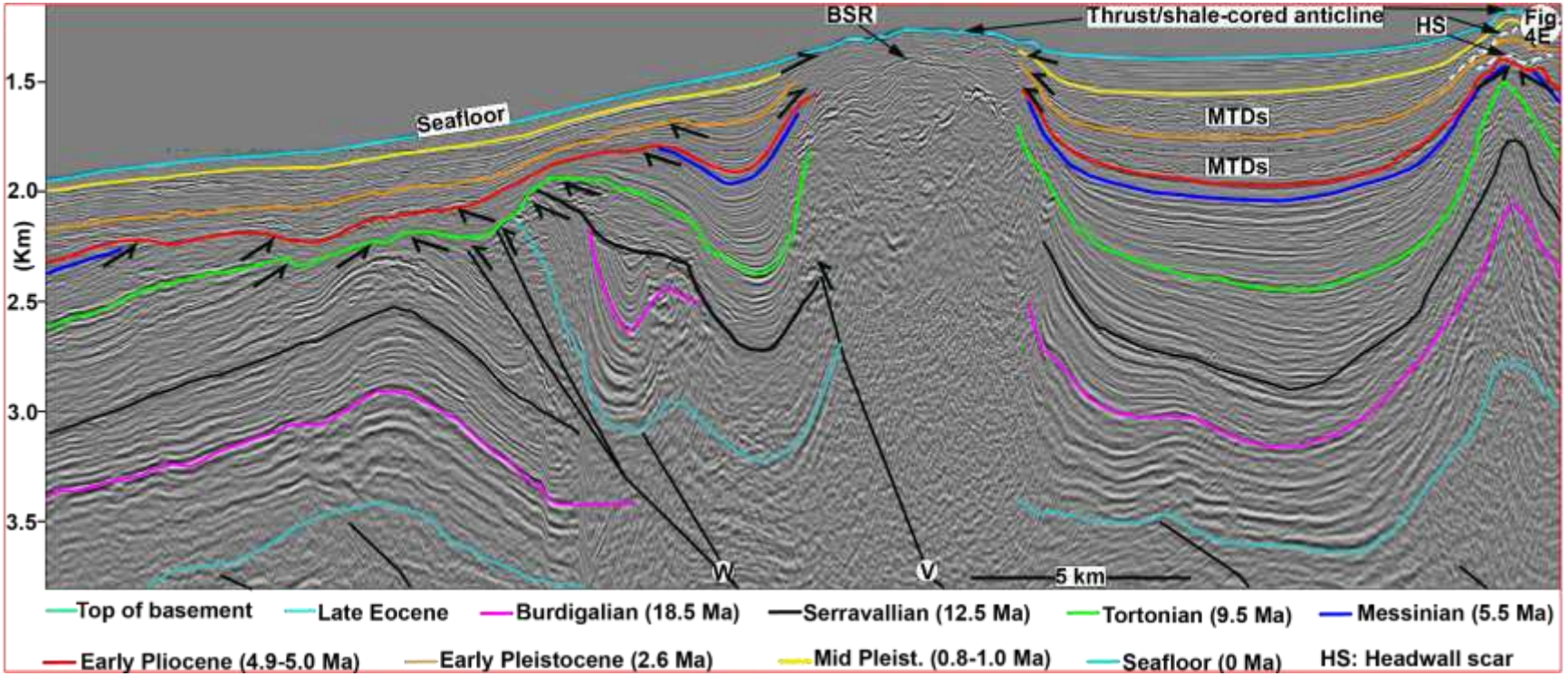

Fig. 4E. Detailed view of the IFTB, showing thrust/shale-cored anticlines, flanked by piggyback/intraslope basins. Note; (i) the presence of headwall scars above the bathymetric surface to the right, that are flanked by MTDs, (ii) the general thinning of stratigraphy above bathymetric high, and a corresponding thickening within piggyback basins, and (iii) the incisional character of the Tortonian, early Pliocene and early Pleistocene surfaces above bathymetric high to the left

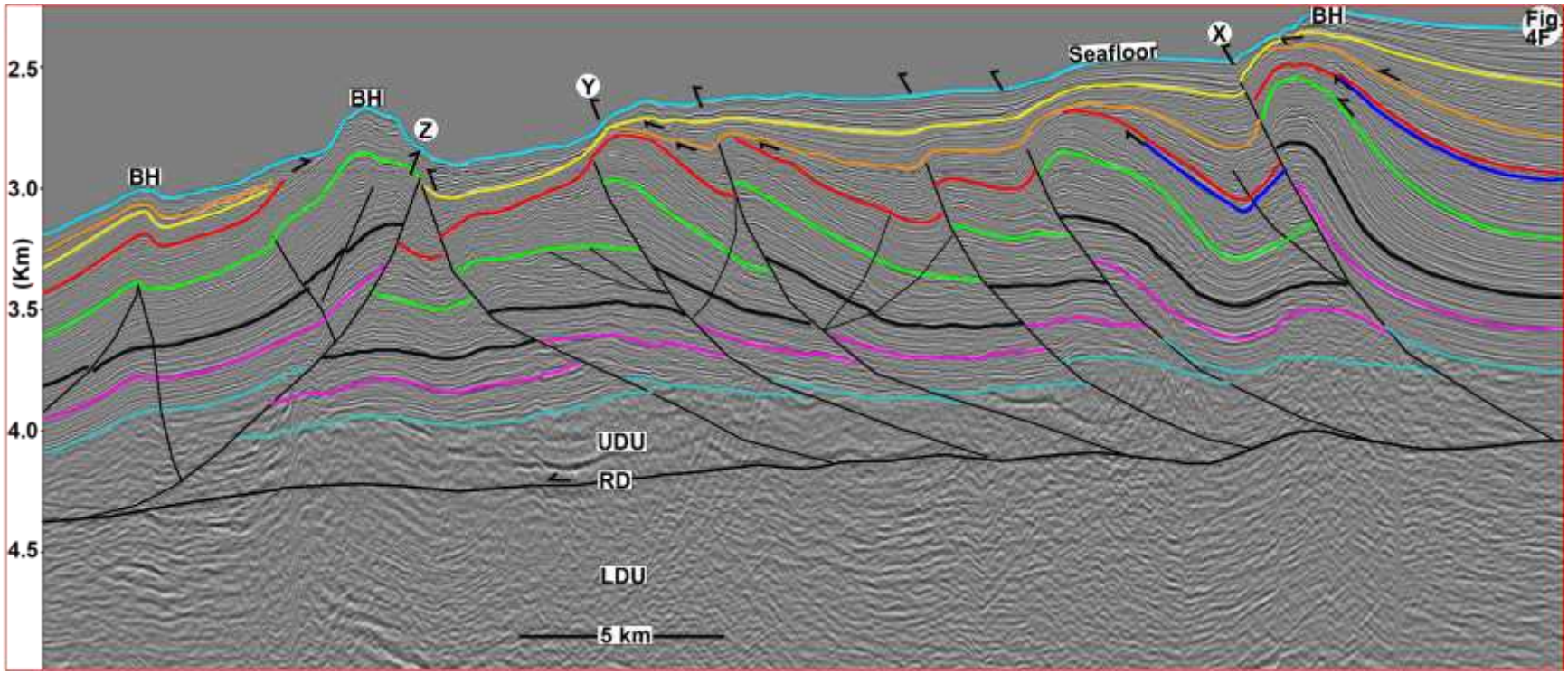

Fig. 4F. Detailed view of the OFTB, showing (i) the detachment of reverse faults on RD, (ii) a general thinning/onlapping of stratigraphy above thrust/shale-cored anticlines, and a corresponding thickening within piggyback basins, (iii) the incisional character of the early and middle Pleistocene surfaces. See text for a more detailed explanation.

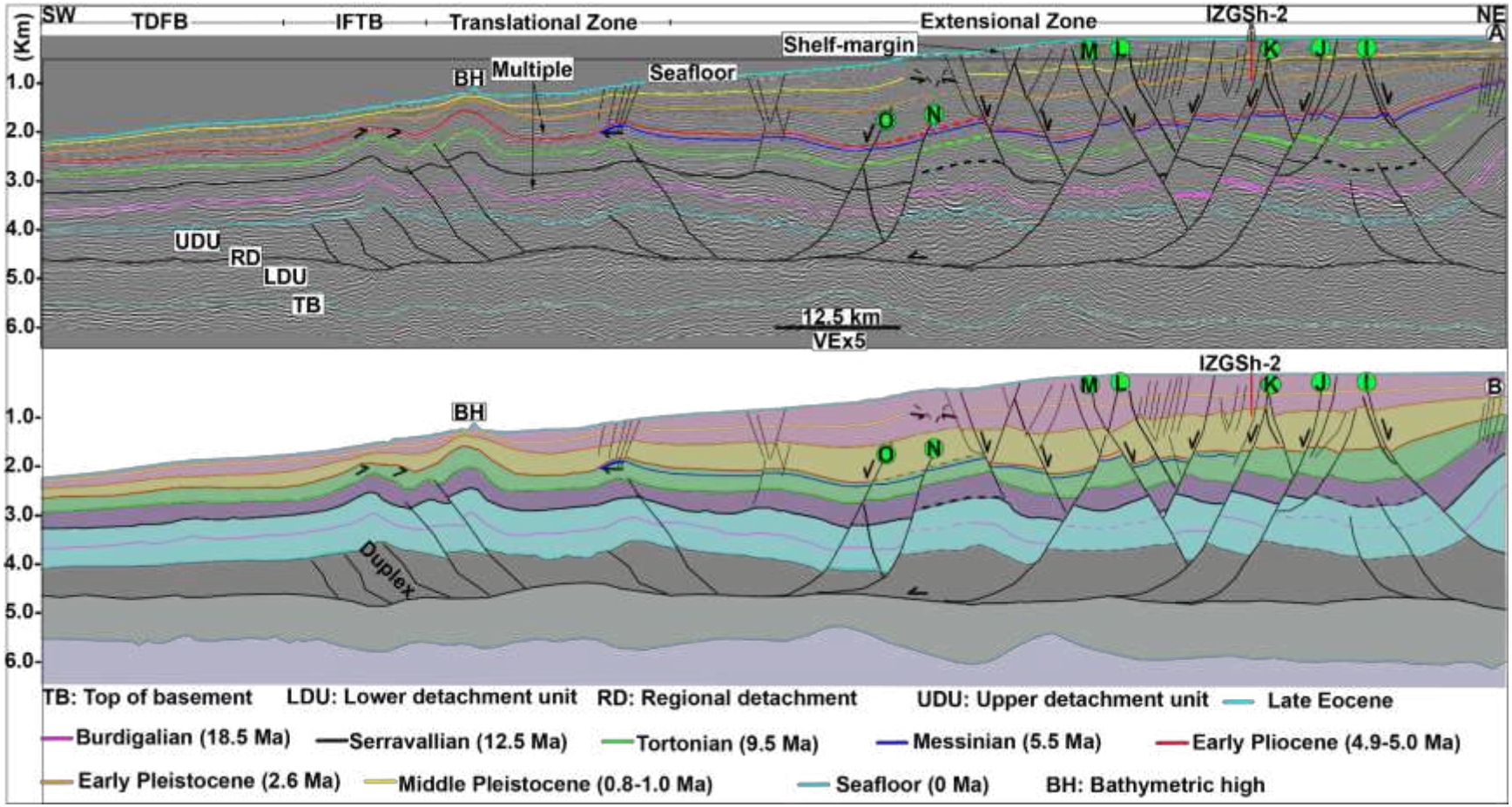

Fig. 5. A, B: Interpreted regional seismic line and line drawing (depth) (see Fig. 1B for location). Note; (i) the listric geometry of normal faults within deeper stratigraphic intervals, and their general termination on RD, (ii) undulating geometry of late Eocene to early Pleistocene surfaces, (iii) a general increase in sediment thickness within the extensional zone from the early Pliocene to present. See text for a more detailed explanation.

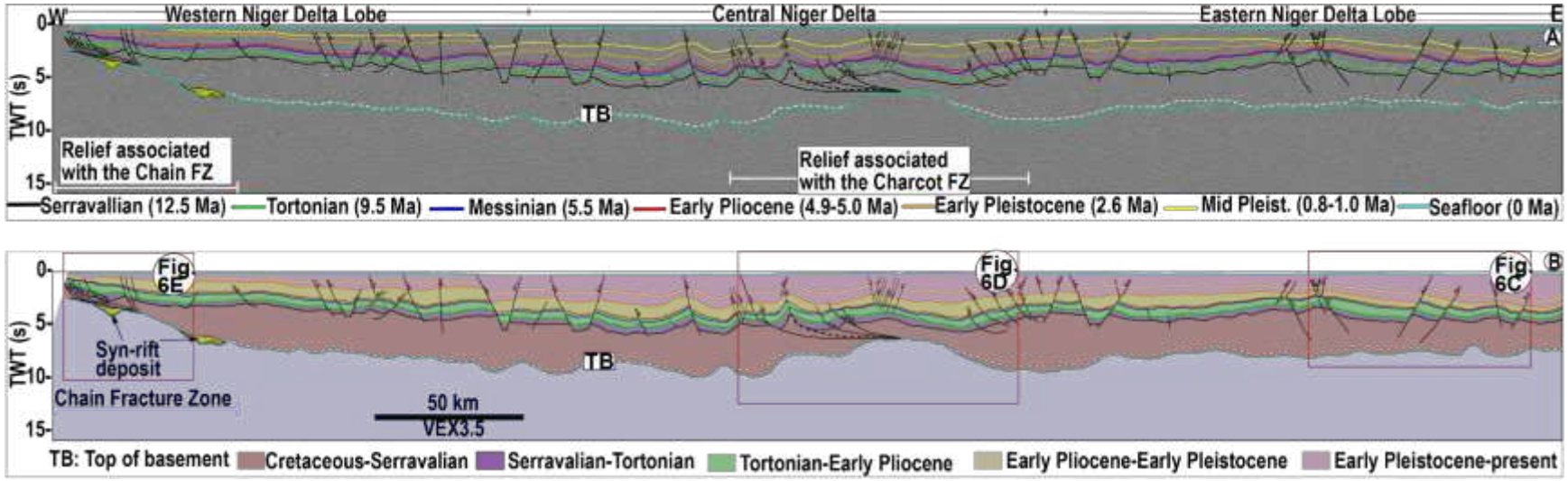

Fig. 6A, B: Interpreted and seismic line drawing of the delta-wide strike line (TWT), located on the shelf (Fig. 1B). Note; (i) the presence of paleo-topographies, formed by the Charcot and Chain Fracture Zones in the central and western Niger Delta, respectively, and the occurrence of listric normal faults above them, (ii) lateral variation in sediment thickness over the Cretaceous-Serravallian, with overall thinning above the relict fracture zones, and thickening on the flanks, the general thinning of the early Pliocene-present Unit from the ENDL to WNDL. For more details, see below, zoomed sections of the areas outlined in red boxes in panel B (Fig. 6C, D and E).

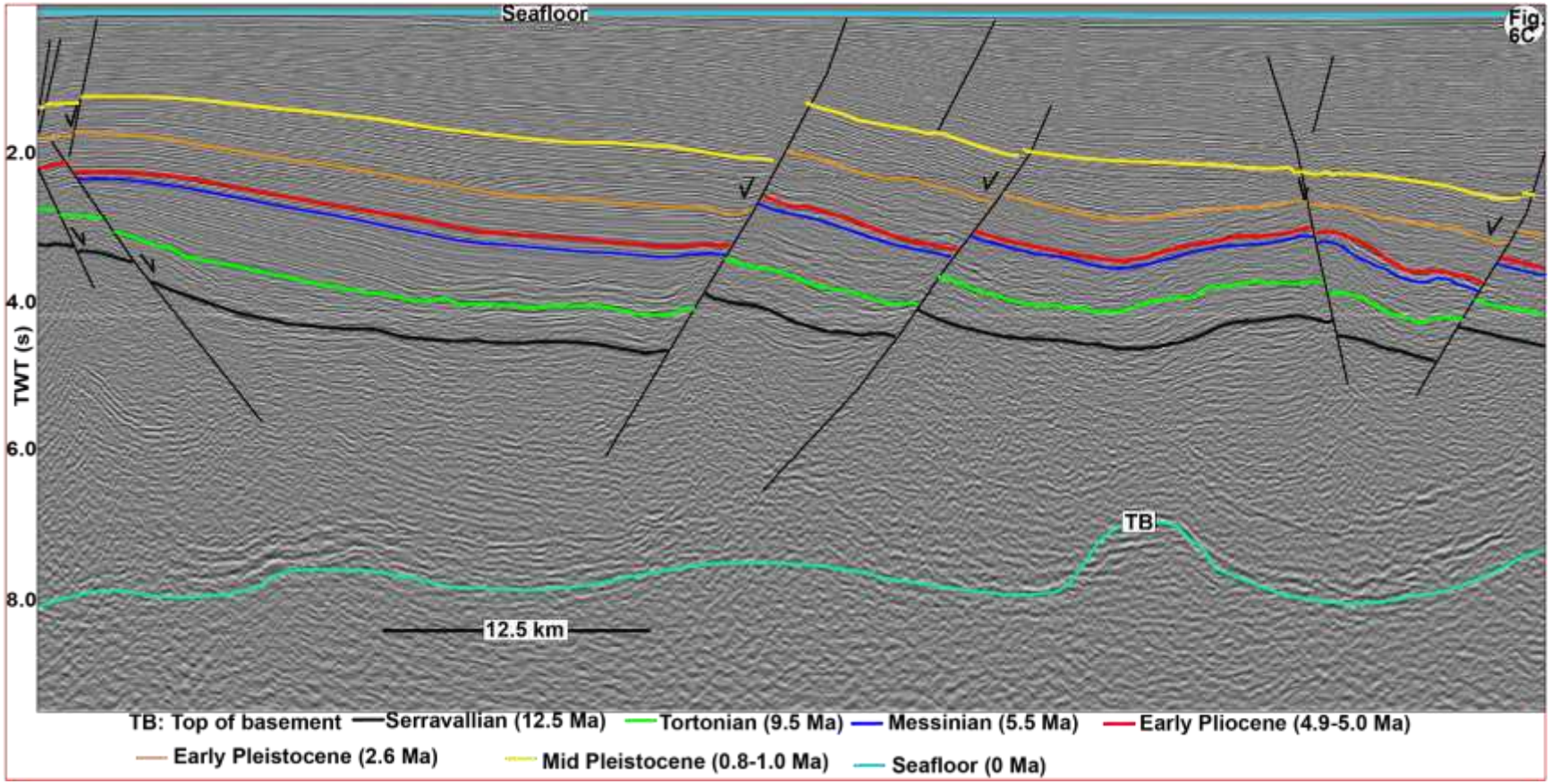

Fig. 6C. Detailed view of the ENDL, showing an overall thickening of the early Pliocene-present Unit.

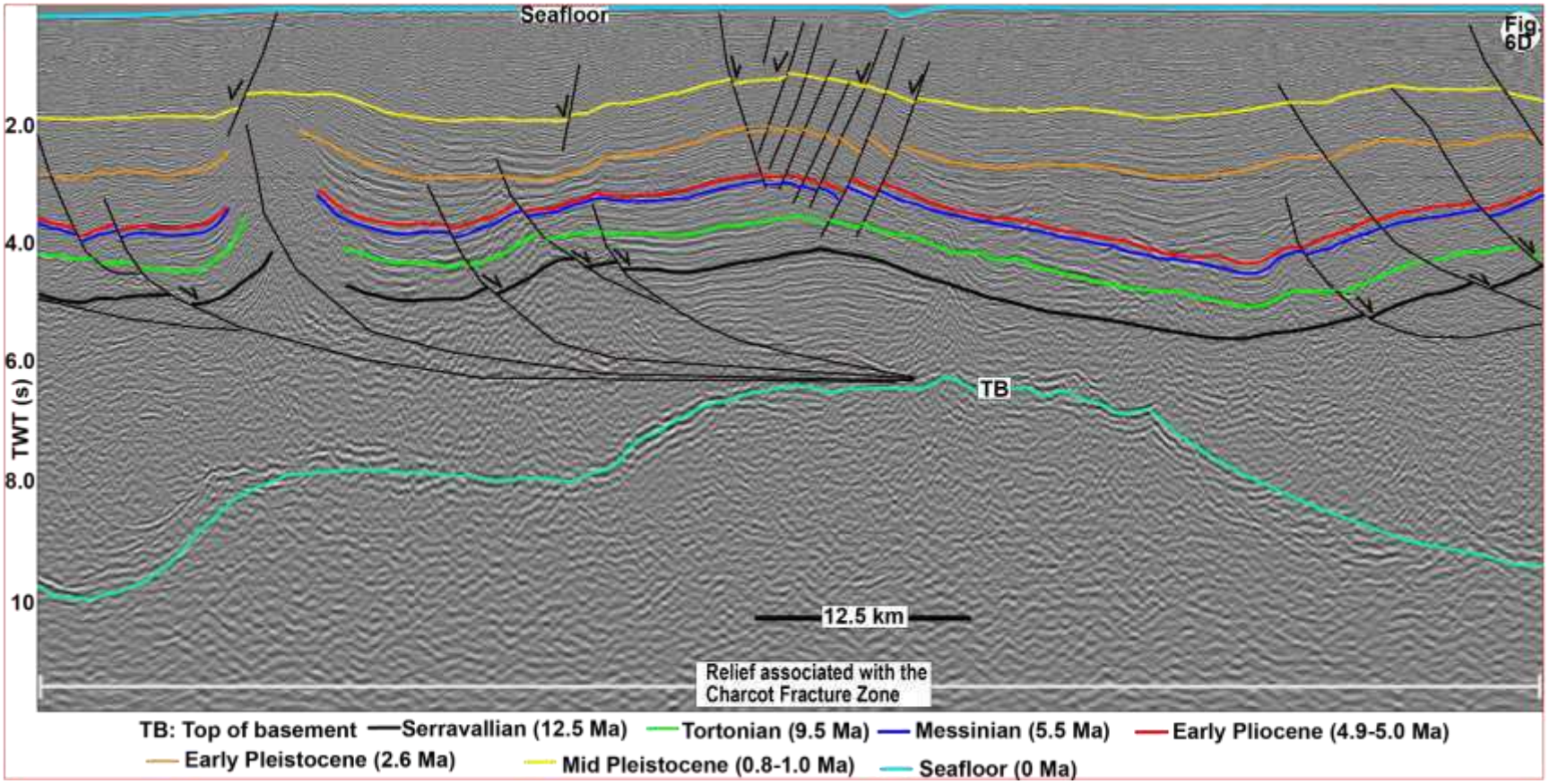

Fig. 6D. Detailed view of the relief, formed by the relict Charcot Fracture Zone. Note the presence of listric normal faults, and an overall thinning of the Cretaceous-Serravallian Unit above the paleo-transform.

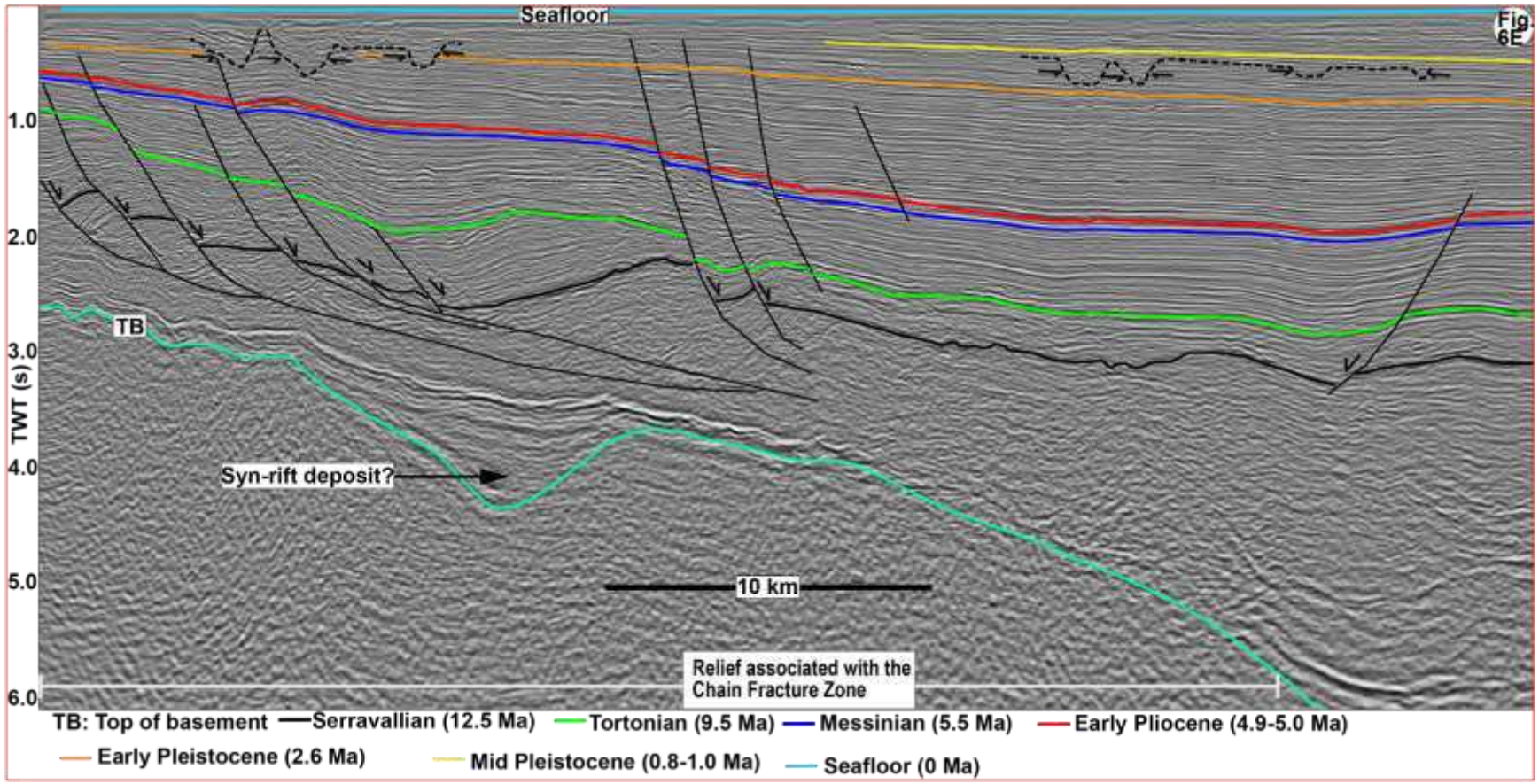

Fig. 6E. Detailed view of the relief, formed by the relict Chain Fracture Zone in the WNDL. Note the presence of listric normal faults, and an overall thinning of stratigraphy above the paleo-transform.

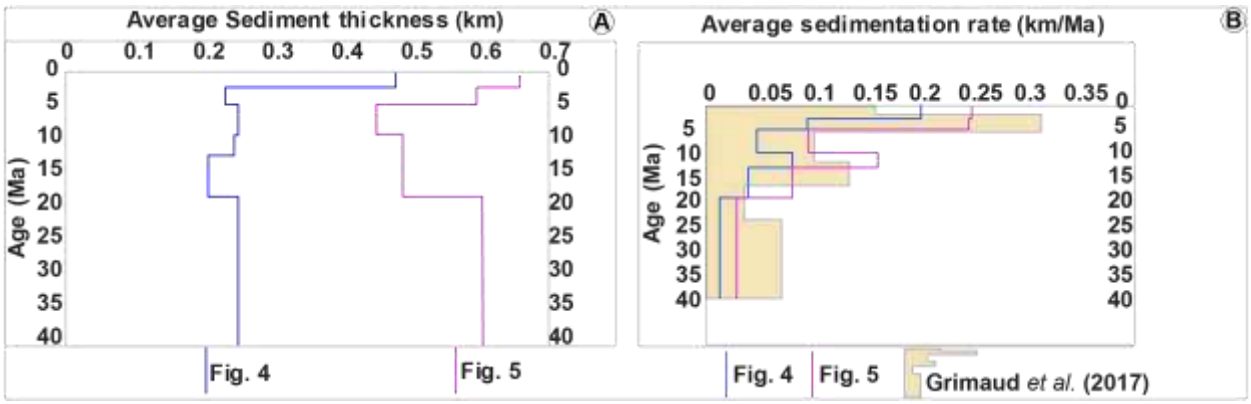

Fig. 7. A, B: Estimated average sediment thickness (km), and sedimentation rates (km/Ma) on the offshore WNDL. Note the general increase in average sediment thickness/deposition rate from the late Eocene to the Tortonian, slight decrease from the Tortonian to the early Pliocene, and onwards increase from the early Pliocene to present.

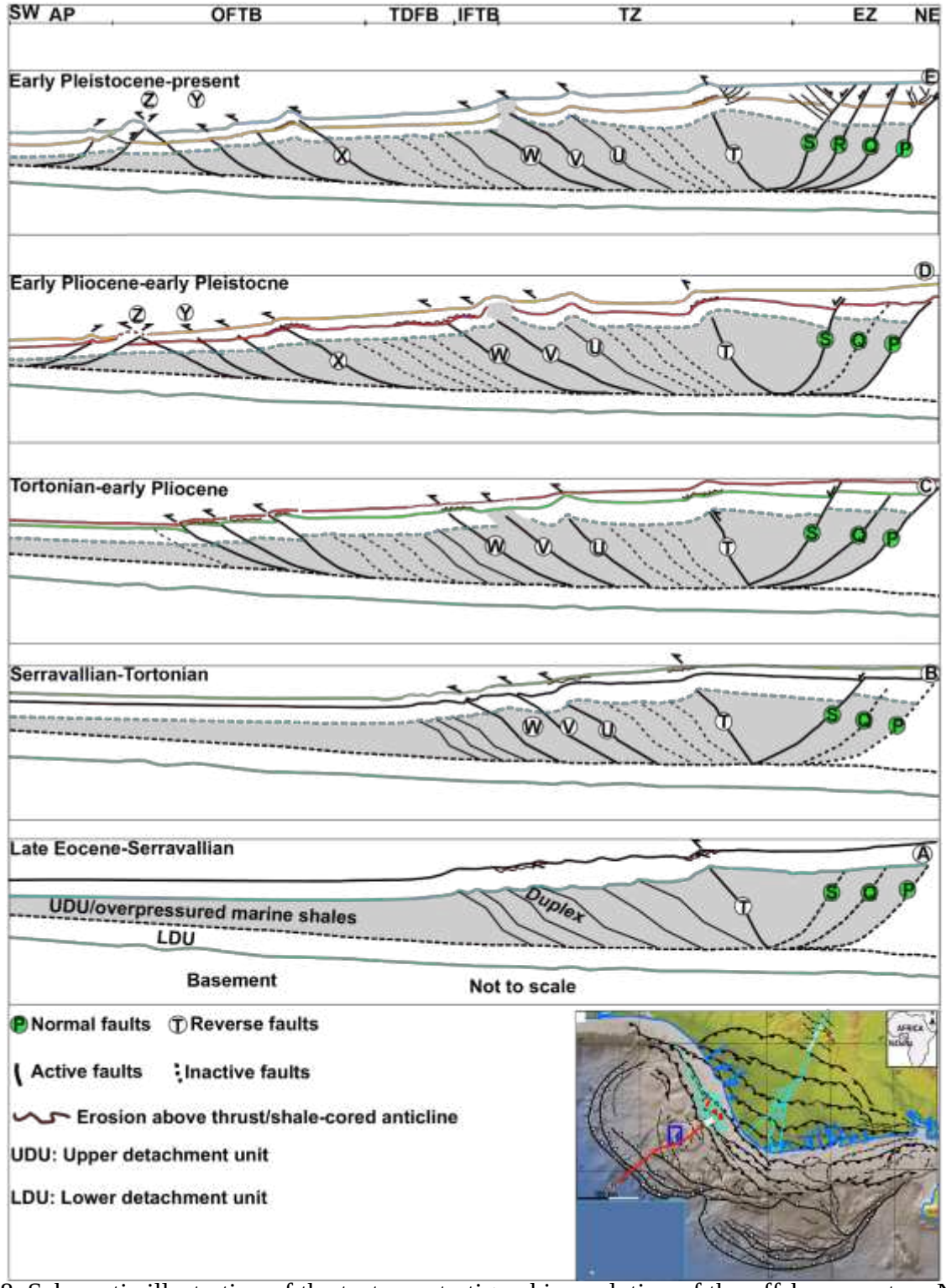

Fig. 8. Schematic illustration of the tectono-stratigraphic evolution of the offshore western Niger Delta from the Cretaceous to the Present. A: Development of duplexes within the upper detachment unit; B: initiation of gravity-driven deformation within the currently active extensional

and translational zones; C: coupling of deformation between the extensional and translational zones, and inferred progradation of the 'Oligocene-Tortonian extensional zone'; D: acceleration of gravity-collapse of the continental shelf, and initiation of deformation within the OFTB; E: intensification of gravity collapse and deformation at the leading front of the OFTB.

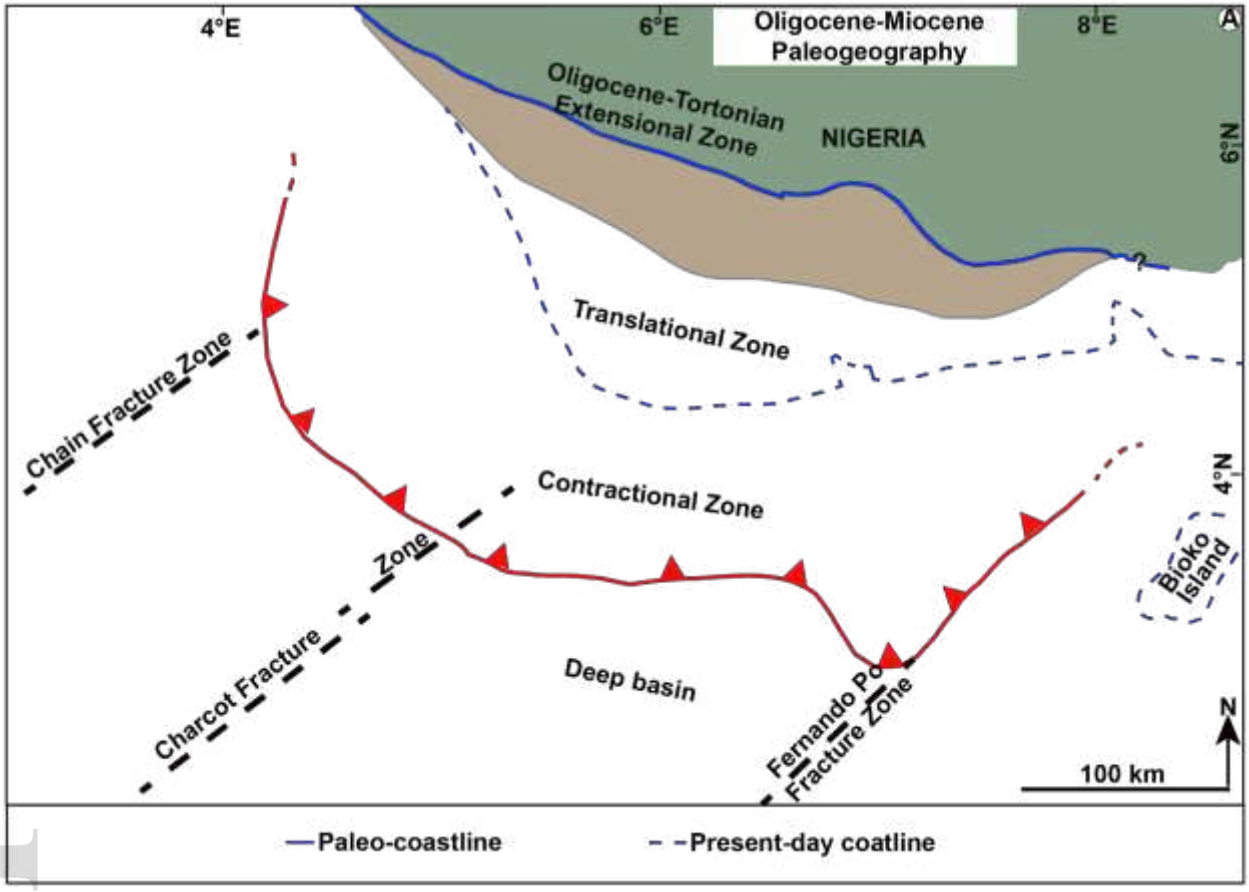

Fig. 9A. Location of the 'Oligocene-Tortonian extensional zone' on the present onshore.

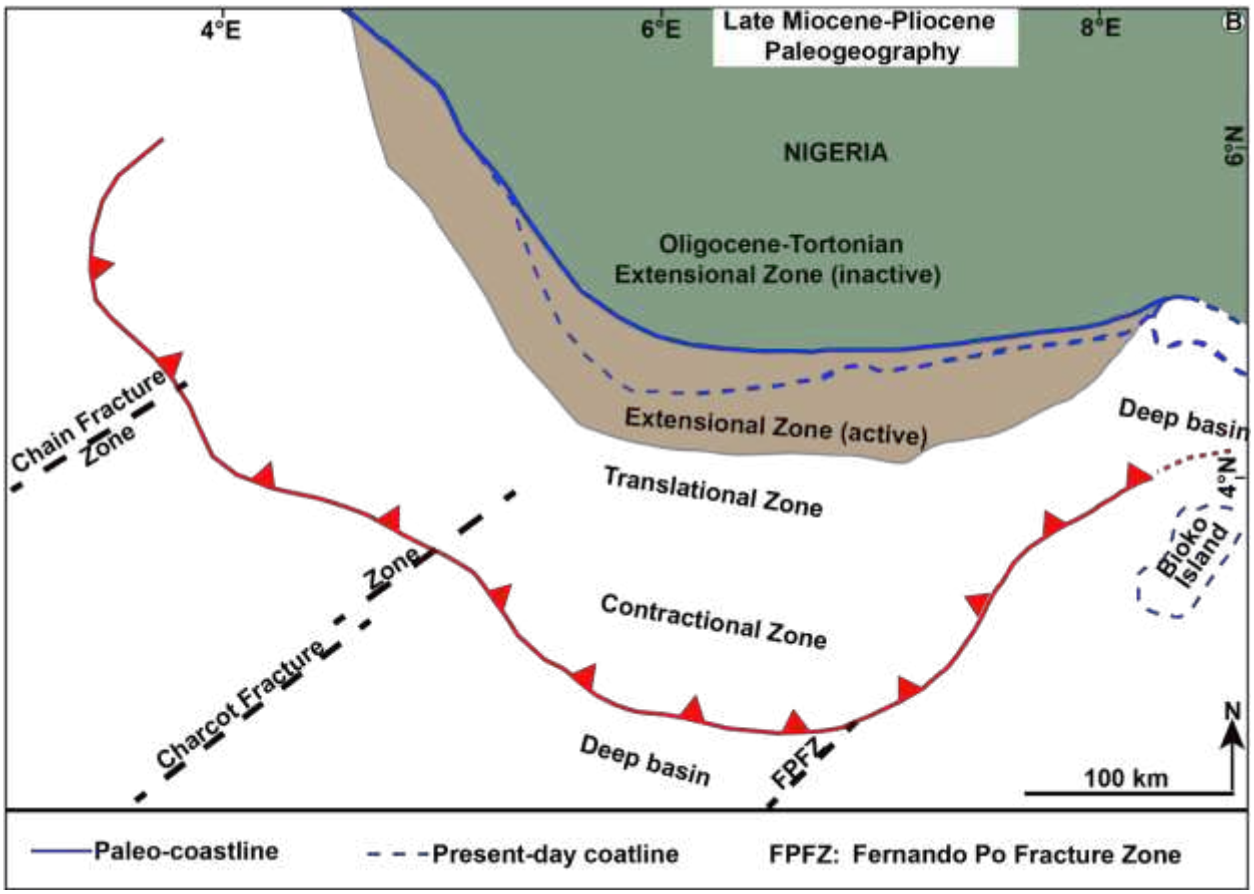

Fig. 9B. Basinward progradation of the 'Oligocene-Tortonian extensional zone'.

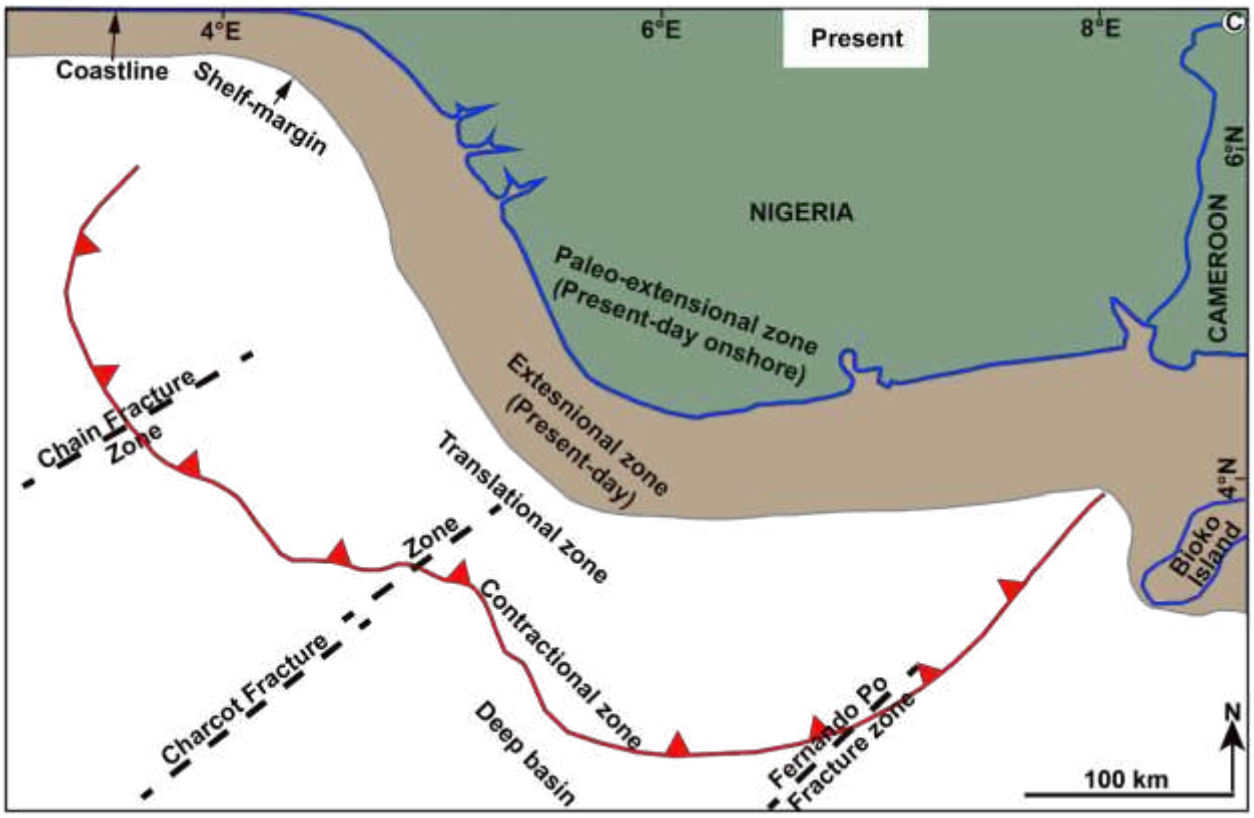

Fig. 9C. Modern Niger Delta extensional, translational and contractional zone.

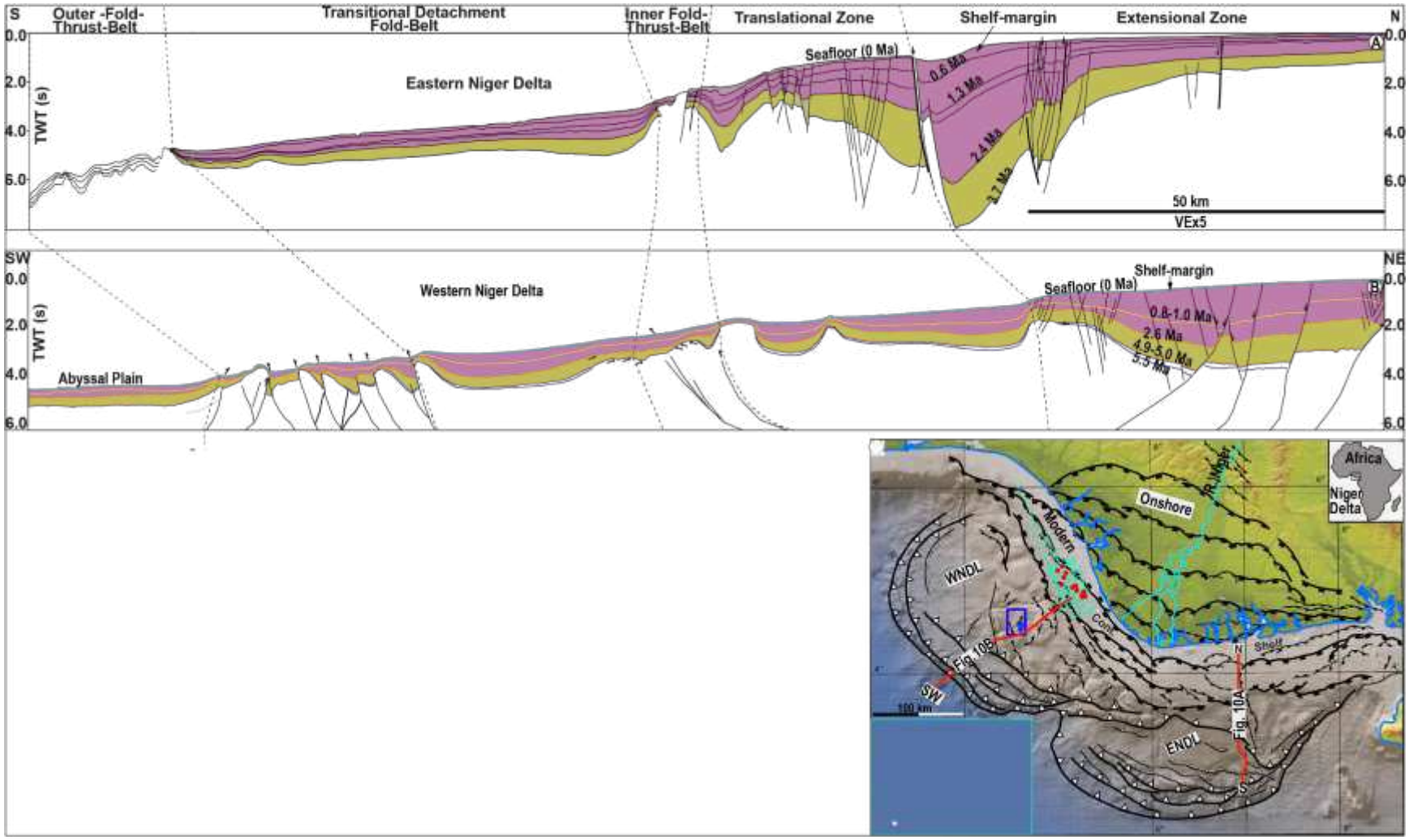

Fig. 10. A, B: Line drawing, showing the stratigraphic architecture of the offshore ENDL (after Jermannaud et al., 2010) and WNDL. Note; (i) Overall progradation during the late and early Pliocene, in the ENDL and WNDL; (ii) retrogradation and sediment storage on shelf of the ENDL in the Pleistocene, compared to progradation and sediment bypass on the shelf of WNDL during the Pleistocene.